Traffic

doi:10.1111/tra.12282

An Actin Filament Population Defined by the Tropomyosin Tpm3.1 Regulates Glucose Uptake

Anthony J. Kee[1], Lingyan Yang[1], Christine A. Lucas[1], Michael J. Greenberg[2], Nick Martel[3], Gary M. Leong[3,4], William E. Hughes[5], Gregory J. Cooney[5], David E. James[6], E. Michael Ostap[2], Weiping Han[7], Peter W. Gunning[8†] and Edna C. Hardeman[1*†]

[1]Cellular and Genetic Medicine Unit, School of Medical Sciences, UNSW Australia, Sydney, NSW 2052, Australia
[2]The Pennsylvania Muscle Institute and Department of Physiology, Perelman School of Medicine at the University of Pennsylvania, Philadelphia, PA 19104-6085, USA
[3]Obesity Research Centre, Institute for Molecular Bioscience, The University of Queensland, St Lucia, QLD 4072, Australia
[4]Department of Paediatric Endocrinology and Diabetes, Mater Children's Hospital, South Brisbane, QLD 4010, Australia
[5]Diabetes and Obesity Program, Garvan Institute of Medical Research, Sydney, NSW 2010, Australia
[6]Charles Perkins Centre, School of Molecular Bioscience, University of Sydney, Sydney, NSW 2006, Australia
[7]Singapore Bioimaging Consortium, Agency for Science, Technology and Research (A*STAR), Singapore, 138667, Singapore
[8]Oncology Research Unit, School of Medical Sciences, UNSW Australia, Sydney, NSW 2052, Australia
*Corresponding author: Edna C. Hardeman, e.hardeman@unsw.edu.au

Abstract

Actin has an ill-defined role in the trafficking of GLUT4 glucose transporter vesicles to the plasma membrane (PM). We have identified novel actin filaments defined by the tropomyosin Tpm3.1 at glucose uptake sites in white adipose tissue (WAT) and skeletal muscle. In Tpm 3.1-overexpressing mice, insulin-stimulated glucose uptake was increased; while Tpm3.1-null mice they were more sensitive to the impact of high-fat diet on glucose uptake. Inhibition of Tpm3.1 function in 3T3-L1 adipocytes abrogates insulin-stimulated GLUT4 translocation and glucose uptake. In WAT, the amount of filamentous actin is determined by Tpm3.1 levels and is paralleled by changes in exocyst component (sec8) and Myo1c levels. In adipocytes, Tpm3.1 localizes with MyoIIA, but not Myo1c, and it inhibits Myo1c binding to actin. We propose that Tpm3.1 determines the amount of cortical actin that can engage MyoIIA and generate contractile force, and in parallel limits the interaction of Myo1c with actin filaments. The balance between these actin filament populations may determine the efficiency of movement and/or fusion of GLUT4 vesicles with the PM.

Keywords actin cytoskeleton, glucose uptake, GLUT4, myosins, tropomyosin

Received 10 August 2014, revised and accepted for publication 11 March 2015, uncorrected manuscript published online 18 March 2015, published online 29 April 2015

Insulin-stimulated glucose uptake in muscle and adipose tissue requires the movement of the glucose transporter, GLUT4, from intracellular storage vesicles (GSVs) to the cell membrane through an exocytotic pathway. The actin cytoskeleton has long been recognized as critical for GLUT4 vesicle trafficking and fusion with the surface membranes of adipocytes and striated muscle (1–4). Insulin stimulation of muscle and fat cells leads to a rapid remodeling of the cortical actin cytoskeleton, and disruption of this remodeling with actin-depolymerizing (Cytochalasin D and Latrunculin A/B) and -stabilizing (Jasplakinolide) drugs inhibits GLUT4 trafficking and glucose uptake (1–4). Numerous studies indicate that actin is involved in the later steps of the pathway, particularly

†These authors contributed equally to this work.

the immobilization of GSVs at or near the plasma membrane (PM) via the exocyst complex (5–10). However, the composition of these actin filaments, how their structure and dynamics are regulated and what precise role they play in the exocytotic process are largely unknown.

We and others have shown in mammalian cells that tropomyosin (Tpm) isoforms define the functional diversity of the actin filament network (11–18). Tpms can increase filament stiffness, protect filaments from the depolymerizing effects of ADF/cofilin and gelsolin (19–21) and influence myosin motor recruitment (11,22) and mechanochemistry (23–25). There is now clear evidence that specific differences between Tpm isoforms account for their differential impact on actin filament function.

Tpm3.1 (Tm5NM1) (see 26 for the new Tpm isoform nomenclature) promotes the inactivation of ADF–cofilin by phosphorylation leading to displacement of ADF–cofilin from the actin filament (11). In addition, incorporation of Tpm3.1 into stress fibers in rat cortical neuronal cells leads to the specific recruitment of non-muscle myosin IIA motors, but not IIB motors, which promotes the contractility and stability of actin filaments (11). In contrast, a Tpm that induces lamellipodia, Tpm1.12 (TmBr3), leads to a reduction in active myosin II levels (11). Pelham et al. (27) showed that the expression of Tpm1.7 (Tm3), but not Tpm3.1, in NRK cells leads to dramatic retrograde transport of myosin I motors and organelles to the perinuclear region. In addition, Tpm2.1 (Tm1), Tpm1.6/1.7 (Tm2/3) and Tpm3.1 stabilized actin filaments at distinct stress fiber regions, whereas Tpm4.1 (Tm4) promoted stress fiber assembly by recruiting myosin II to stress fiber precursors. Elimination of any one of the Tpms fatally compromises stress fiber formation (22).

The specificity of Tpm isoform function is also true in yeast where acetylation of the single Tpm protein results in distinct Tpm species. One Tpm isoform has been shown to inhibit the interaction of actin with myosin I motors (MyoIp), but favor the association (and ATPase activity) of myosin V motors (Myo51p and Myo52p) with actin filaments (28). Furthermore, yeast uses the sorting of Tpm isoforms to regulate the recruitment of myosin II, but not myosin V, to the contractile ring in dividing cells (25,29–31). In addition, recent studies in yeast have demonstrated that the actin nucleators, the formins, dictate which Tpm isoforms are incorporated into growing actin filaments and consequently specify the functional properties of the actin filaments they generate (32).

We previously described a population of cytoskeletal actin filaments in skeletal muscle fibers defined by the Tpm isoform Tpm3.1 that is located at the sarcolemma and T-tubule membrane (15,33), sites of glucose uptake in this tissue. Here we show that manipulation of this Tpm in transgenic (Tg) and knockout (KO) mice impacts on glucose clearance into skeletal muscle and epididymal white adipose tissue (WAT). Studies in 3T3-L1 adipocytes show that Tpm3.1 alters insulin-dependent glucose uptake by regulating the accumulation of the GLUT4 glucose transporter at the PM. Inhibition of Tpm3.1 using a novel anti-Tpm drug prevents (41) insulin-stimulated translocation of GLUT4 to the PM. Furthermore, Tpm3.1 regulates actin filament levels and components of the exocyst complex in WAT including Myo1c that has been shown to regulate GLUT4 levels in the PM. Consistent with previous reports in other cell systems (11) we find here that Tpm3.1 localizes with MyoIIA in differentiated adipocytes. Additionally, we find that this Tpm inhibits Myo1c binding and restricts significant gliding of the motor. We propose that Tpm3.1 determines the number of cortical actin filaments that can engage MyoIIA and generate local contractile force, and in parallel limits the number of actin filaments that can interact with Myo1c. Consequently, we propose that the balance between these actin filament populations determines the efficiency of movement and fusion of GLUT4 vesicles with the PM.

Results

Tpm3.1 protects against the effects of high-fat feeding

To understand the role of Tpm3.1 in the maintenance of glucose homeostasis we performed glucose and insulin tolerance tests (GTT and ITT) on Tpm3.1 homozygous KO and wild-type (WT) control mice maintained on normal chow (8% energy as fat) or 9 weeks of high-fat diet (HFD) feeding (45% energy as fat) (Figure S1A–D, Supporting Information and Figure 1A–D, respectively). In mice maintained on normal chow, glucose clearance was similar in KO compared with WT mice (Figure S1A); there was no significant difference in area-under-the-curve (AUC) for

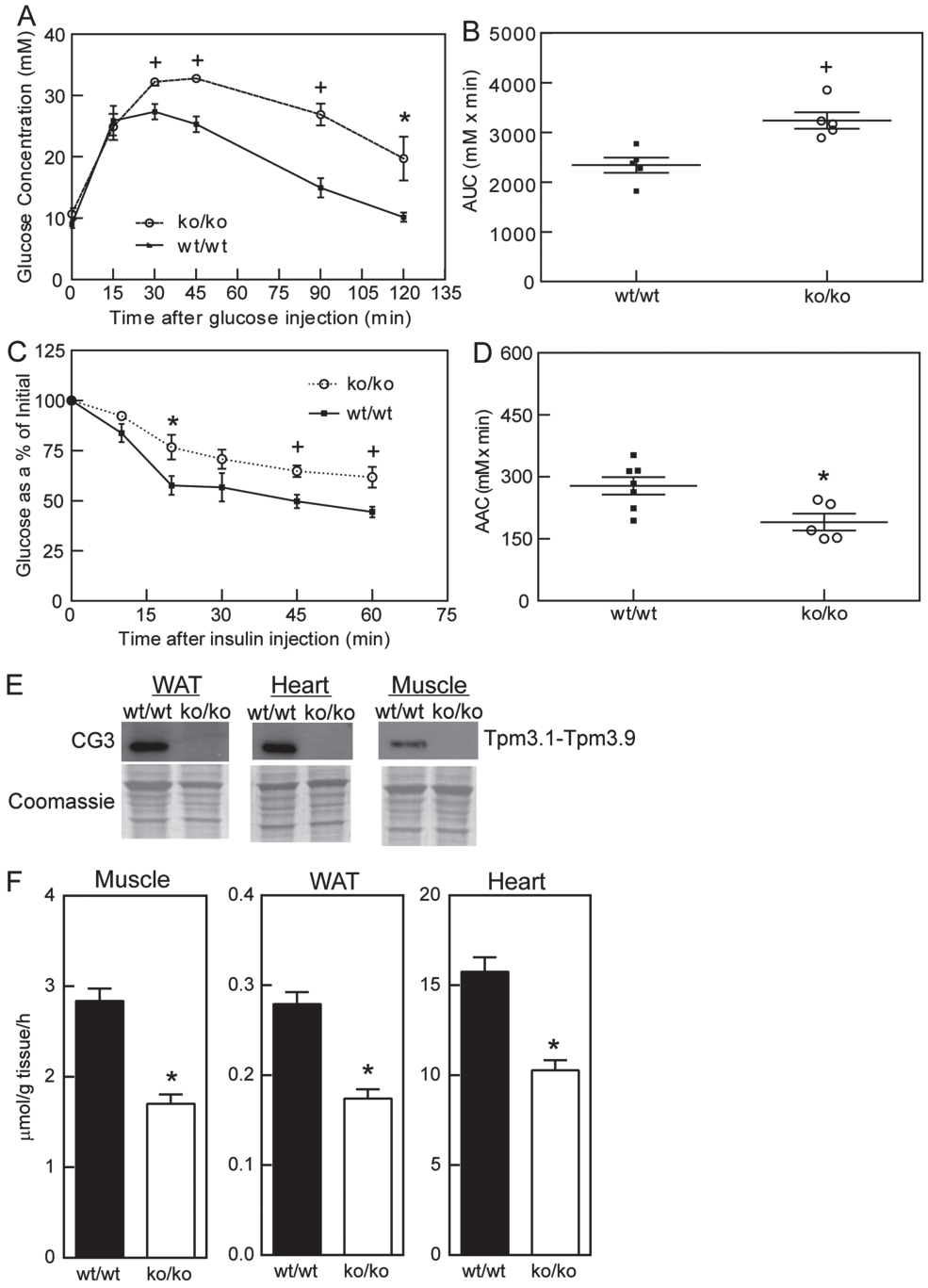

Figure 1: Legend on next page.

glucose clearance between WT and KO mice (Figure S1B). Insulin sensitivity was also unchanged in the KO mice, there being no difference in the area-above-the-curve (AAC) for ITT between KO and WT mice (Figure S1C,D). After HFD, as expected, WT mice cleared glucose less well than chow-fed mice (AUC normal chow 1564 ± 120 mM min; AUC HFD 2338 ± 153 mM min, $p < 0.05$). Significantly, the HFD had a greater effect on glucose homeostasis in KO than WT mice; the KO mice cleared glucose substantially less well than WT mice (Figure 1A,B) at least in part due to decreased insulin sensitivity (Figure 1C,D).

To determine whether the poor glucose clearance in KO mice on a HFD was due to decreased uptake into insulin-responsive tissues, we measured ^{3}H-2-deoxyglucose (2-DG) uptake into skeletal muscle, epididymal WAT and heart during a GTT (Figure 1F). We first established that expression of Tpm3.1 was absent from these tissues using an antibody (CG3) recognizing all cytoskeletal Tpm isoforms produced by the *Tpm3* gene (including Tpm3.1) (Figure 1E). The absence of a band in the western blots of KO tissue using the CG3 antibody also indicated that no other cytoskeletal isoforms from the *Tpm3* gene (Tpm3.3–3.9) were expressed to compensate for the absence of Tpm3.1. Uptake of 2-DG into skeletal muscle, WAT and heart was significantly decreased in HFD-fed KO compared with HFD-fed WT mice (Figure 1F). Together these data indicate that loss of Tpm3.1 increased the sensitivity of mice to the detrimental effects of HFD feeding on glucose clearance in skeletal muscle, WAT and heart.

Tpm3.1 promotes increased glucose clearance and glucose uptake into insulin-responsive tissues

We examined glucose metabolism in normal chow-fed Tg mice expressing human Tpm3.1 under the control of the β-actin promoter (11). In this mouse, there was a 3.5-, 6.3- and 4.2-fold increase in Tpm3.1 protein levels above endogenous in WAT, heart and skeletal muscle, respectively (Figure 2A). Glucose clearance was increased in heterozygous Tpm3.1 Tg mice (Figure 2B). This was reflected as a significant decrease in AUC of the GTT in Tg compared with WT littermate controls (Figure 2C). To examine whether the increased clearance was due to increased insulin sensitivity we then performed ITTs. These tests showed that the Tg mice cleared glucose more rapidly than the WT mice in response to the insulin injections (Figure 2D) resulting in a significantly increased AAC for the Tg versus WT mice (Figure 2E). The increased glucose clearance and insulin sensitivity were also observed in mice of a different genetic background (FVB/N versus C57Bl/6). Figure S2A,B shows a dose-dependent impact of the Tpm3.1 transgene on glucose clearance in a GTT on the FVB genetic background. Increased clearance was also observed in an ITT on the FVB background (Figure S2C,D). We also tested whether the effect of Tpm3.1 was due to overexpression of a Tpm *per se* by examining glucose clearance in a Tg mouse line expressing an unrelated Tpm isoform, Tpm1.7 (Tm3), in muscle (33) and WAT (Figure 3A). In this mouse line, there was no impact on glucose clearance compared with WT controls (Figure 3B,C), providing support that the effect on glucose clearance is not simply due to Tpm overexpression, but is specific to Tpm3.1.

We examined glucose uptake in the tissues of the Tpm3.1 Tg mice. 2-DG uptake in skeletal muscle, WAT and heart of these mice during a GTT was significantly increased compared with WT controls (Figure 2F). This was at least in part due to increased insulin sensitivity in these tissues as 2-DG uptake was also increased in the Tg mice during an ITT (Figure 2G). Taken together, the data demonstrate that Tpm3.1 can positively regulate glucose uptake in mouse tissues.

Tpm3.1 has little impact on animal activity or whole body oxidative metabolism

Food intake, activity (ambulatory movements) and whole body oxidative metabolism (O_2 consumption and respiratory exchange ratio, RER) were measured in Tg and KO mice by indirect calorimetry. In the Tg mice on normal chow, food intake, O_2 consumption and

Figure 1: Tpm3.1 protects against the effect of high-fat feeding on glucose clearance in WAT, heart and skeletal muscle. A) GTT and (B) AUC of the GTT for 16-week-old Tpm3.1 KO (ko/ko) and WT (wt/wt) mice fed a HFD (45% energy as fat) for 16 weeks showing decreased glucose clearance in KO mice ($n = 5$/group). C) ITT (1.5 U/kg body weight) and (D) AAC of the ITT for 16-week-old mice fed a HFD for 16 weeks showing decreased insulin sensitivity in KO mice ($n = 5$/group). E) Western blots of WAT, heart and skeletal muscle from WT and KO mice using the CG3 antibody that recognizes all cytoskeletal Tpm isoforms from the *Tpm3* gene (Tpm3.1–Tpm3.9). Lack of a band in the KO tissues indicates that other cytoskeletal isoforms from the *Tpm3* gene are not being expressed to compensate for the lack of Tpm3.1. F) ^{3}H-deoxyglucose uptake during a GTT in WAT, heart and skeletal muscle of 16-week-old WT and KO mice fed a HFD for 9 weeks showing decreased glucose uptake in tissues from the KO mice ($n = 5–6$/group). Data are mean ± SEM. Statistical significance is indicated by *$p < 0.05$ and +$p < 0.01$ (Mann–Whitney *U* test).

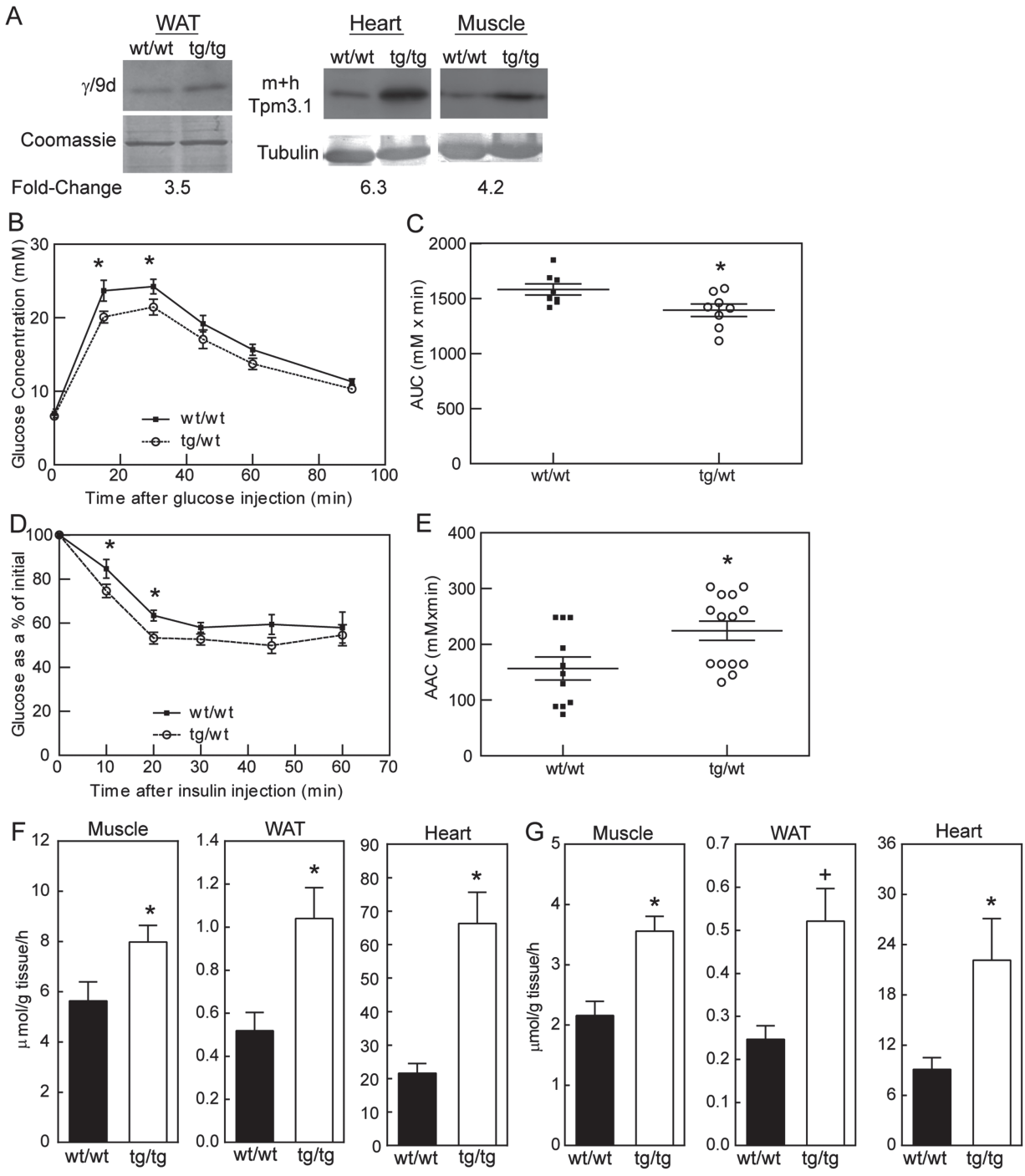

Figure 2: Legend on next page.

ambulatory activity were unchanged compared with WT mice (Figure S2E–G). There was also no difference in food intake, either normal chow or HFD, in the KO compared with WT mice (Figure S1E). Consumption of a HFD produced an expected decrease in RER compared with normal chow (0.810 ± 0.006 versus 0.903 ± 0.001, respectively) (Figure S1F), indicating that the mice were utilizing increased amounts of fat for energy requirements. However, there was no difference in oxidative metabolism (RER) or ambulatory activity between the KO and WT

mice (Figure S1F,G, respectively). These data indicate that altered food intake, activity and oxidative metabolism are not responsible for the altered glucose clearance in the Tg mice and the increased sensitivity of the KO mice to the effects of HFD feeding.

Tpm3.1 limits filamentous actin pool size in WAT

The actin cytoskeleton plays a major role in GLUT4 vesicle trafficking, particularly the later tethering and fusion stages of the exocytotic process (4). Tpm3.1 has been shown to alter F-actin pools in primary hippocampal neurons of the Tpm3.1 Tg mouse (34). We therefore determined if altered levels of Tpm3.1 regulate actin filament levels in WAT of these mice. Compared with WT adipocytes, we detected a 30% increase ($p = 0.019$) and a 15% decrease ($p < 0.001$) in filamentous actin (detected with phalloidin) in the cell cortex of Tg and KO adipocytes, respectively (Figure 4A,B). This occurred without significantly altering the total levels of actin in the Tg and KO WAT (Figure 4C,D); although, an indication of an increase ($p = 0.16$) was apparent in the Tg WAT (Figure 4D). However, the increase in filamentous actin in the Tg adipocytes was not unique to overexpression of Tpm3.1. Adipocytes in the Tpm1.7 Tg mice also showed an increased level of filamentous actin (Figure 4E,F), which was similar in level to that seen in Tpm3.1 Tg mice. Thus, while we cannot rule out a potential involvement of altered levels of filamentous actin in regulating GLUT4 trafficking and membrane exposure, it is clear that this process requires a specific actin filament population containing Tpm3.1, but not Tpm1.7.

Tpm3.1 does not affect insulin-stimulated Akt signaling

The main signaling pathway that is responsible for insulin-dependent glucose uptake in skeletal muscle and adipose tissue is the Akt pathway (35,36). Indeed, Akt2 has been shown to be necessary and sufficient for insulin-stimulated glucose uptake in adipocytes (36). To test if altered Akt signaling was responsible for the increase in glucose uptake in the Tpm3.1 Tg mice, we examined insulin-stimulated Akt phosphorylation in WAT and skeletal muscle from these mice. Insulin stimulation (0.5 U/kg body weight, I.P.) led to a robust phosphorylation of Akt (Ser473) in WAT and skeletal muscle that was similar between WT and Tg mice (Figure S3). Total Akt levels were also similar in WT and Tg mice and was unaffected by insulin stimulation (Figure S3). These data show that Tpm3.1's effect on glucose uptake is not via altered Akt phosphorylation, but rather due to impacts on downstream events. The most likely candidate downstream event(s) is the involvement of Tpm3.1-containing actin filaments in the delivery of GLUT4 to the PM. This is consistent with the observed changes in filamentous actin in the Tg and KO adipocytes *in vivo*.

Tpm3.1 colocalizes with GLUT4 in mouse skeletal muscle and WAT

In keeping with Tpm3.1 having a role in glucose uptake, Tpm3.1 was colocalized with GLUT4 in both skeletal muscle and WAT (Figure 5). In skeletal muscle, these two proteins were localized to striated structures (Figure 5A), which were previously defined as T-tubule membranes (15,37), the major sites of glucose uptake (38–40). In WAT, fluorescence intensity line scans across adipocytes revealed regions at the PM where there was significant overlap of Tpm3.1 and GLUT4 (Figure 5B). In 3T3-L1 adipocytes, Tpm3.1 was located diffusely throughout the rest of the cell (Figure 5C). With insulin stimulation, there was a significant increase in Tpm3.1 at the cell cortex (Figures 5C, 6A and 7A). This insulin-dependent change

Figure 2: Tpm3.1 promotes increased glucose clearance and insulin sensitivity in WAT, heart and skeletal muscle. A) Western blots of WAT, heart and skeletal muscle from WT (wt/wt) and homozygous Tpm3.1 Tg (tg/tg) (FVB/N) mice using the γ/9d antibody that recognizes endogenous (mouse, m) and exogenous (human, h) Tpm3.1. Tg mice have a 3.5-, 6.3- and 4.2-fold increase in Tpm3.1 expression in WAT, heart and muscle, respectively. B) GTT and (C) AUC of the GTT for 12-week-old mice on normal chow showing increased glucose clearance in Tpm3.1 Tg (C57Bl/6) mice ($n = 6–8$/group). D) ITT and (E) AAC of the ITT for 12-week-old mice on normal chow showing increased insulin sensitivity of the Tg mice ($n = 11–14$/group). ^{3}H-deoxyglucose uptake during a (F) GTT and an (G) ITT in WAT, heart and skeletal muscle of 12-week-old normal chow-fed WT and Tg (FVB/N) mice showing increased glucose uptake and insulin sensitivity in tissues of the Tg mice ($n = 5$/group). Data are mean ± SEM. Statistical significance is indicated by *$p < 0.05$, +$p < 0.01$ (Mann–Whitney *U* test).

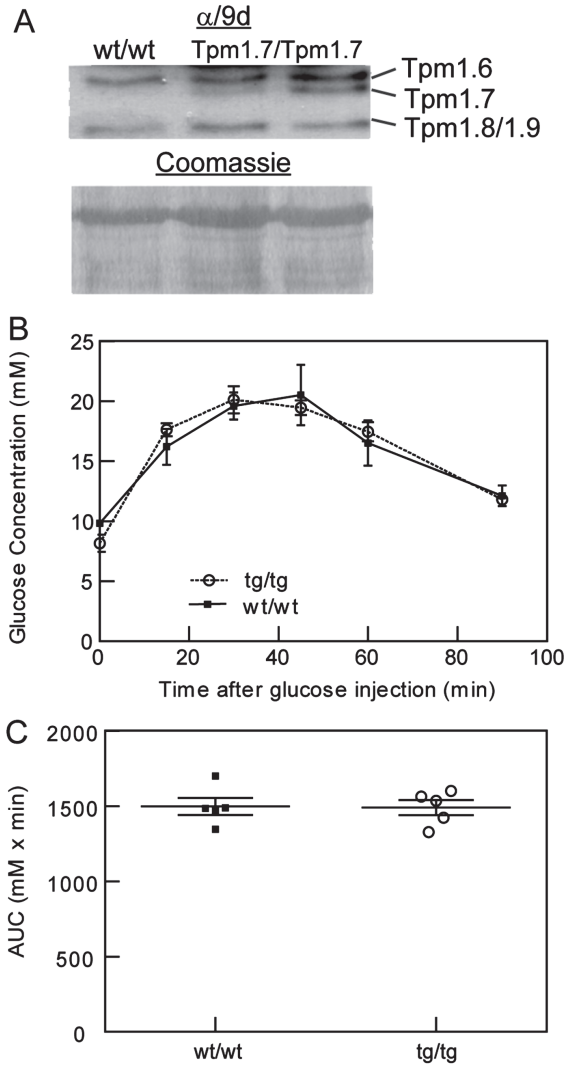

Figure 3: Glucose clearance is not affected in Tpm1.7 Tg mice. A) Western blots showing Tpm1.7 levels in WT and Tpm1.7 Tg mice. B) GTT and (C) AUC of the GTT for 14-week-old mice on normal chow showing no difference in glucose clearance in Tpm1.7 Tg (Tpm1.7/Tpm1.7) mice ($n = 5–6$/group).

in Tpm3.1 localization to the cell cortex is consistent with Tpm3.1 having a role in GLUT4 accumulation at the PM.

Treatment of adipocytes with a Tpm3.1 inhibitor abrogates insulin-stimulated GLUT4 accumulation at the PM and glucose uptake

To more directly investigate the role of Tpm3.1 in glucose uptake we used a novel small molecule inhibitor, TR100. TR100 interacts with Tpm3.1 at its C-terminus and inhibits its ability to stabilize actin filaments (41). Unlike other actin-destabilizing drugs (Cytochalasin or Latrunculin) it does not act on all actin filaments, only those containing Tpm3.1 or Tpms with similar structure (41). In unstimulated cells (no insulin) 1-h treatment with the inhibitor led to a redistribution of Tpm3.1 to the cell cortex, confirming the impact of the inhibitor on Tpm3.1 organization in the cell (Figure 6A). Additionally, TR100 had a major impact on the organization of actin. The inhibitor led to a significant accumulation of F-actin in the cell interior and relative loss at the cell cortex (Figure 6B), consistent with Tpm3.1 having a role in inhibiting actin filament depolymerization (41).

The inhibitor also affected insulin-stimulated GLUT4 translocation to the PM. In the basal state (minus insulin), TR100 had little effect on GLUT4 localization at the cell periphery or in the perinuclear compartment (Figure 6C). As expected, insulin treatment of non-inhibitor-treated cells (DMSO treated) led to a significant increase in GLUT4 at the cell cortex (Figure 6C). However, in the presence of the inhibitor (at 20, 50 and 100 μM), the amount of GLUT4 at the cell periphery during insulin stimulation was dramatically reduced (~75% decrease in insulin-stimulated GLUT4 at the cortex with 50 and 100 μM TR100).

To determine whether this decrease in GLUT4 trafficking to the PM had a functional consequence we measured the impact of TR100 on insulin-stimulated glucose uptake in 3T3-L1 adipocytes. At both 20 and 50 μM, TR100 significantly decreased the rate of insulin-stimulated glucose uptake; there being a 55 and 70% decrease in insulin-stimulated glucose uptake at the two inhibitor doses, respectively (Figure 6D). Importantly, TR100 had no impact on basal glucose uptake (Figure 6D), overall adipocyte morphology (Figure 6A–C) or cell viability (data not shown). This indicates that the effect of TR100 on insulin-stimulated events is not simply due to non-specific toxic effects of the inhibitor. We conclude that Tpm3.1 has a role in regulating insulin-stimulated GLUT4 accumulation at the PM and glucose uptake.

Tpm3.1 colocalizes with MyoIIA and its localization is disrupted by the Tpm3.1 inhibitor

Tpm3.1-containing actin filaments have been shown to recruit MyoIIA motors to actin stress fibers in neuroepithelial cells (11). Here we found that MyoIIA was colocalized

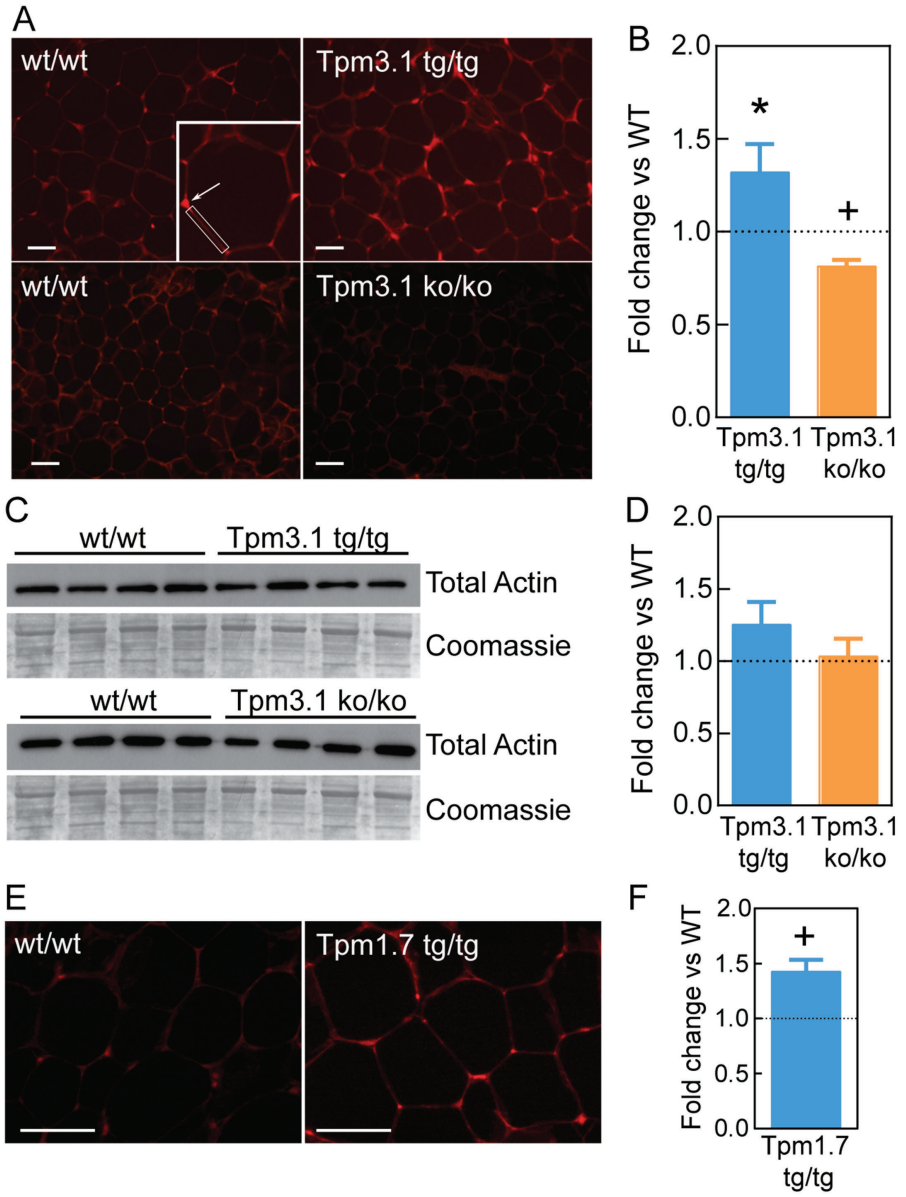

Figure 4: Tpm3.1 regulates the pool size of filamentous actin in WAT. A) Representative images of filamentous actin (F-actin) in WAT from WT, Tpm3.1 Tg and KO mice visualized with phalloidin. Insert in the upper left image is of an adipocyte at higher magnification showing F-actin at the cell cortex (boxed area) and intense signal at the intersection between three adipocytes (arrow) due to blood vessels and stromal cells. Scale bars = 50 μM. B) Quantification of the phalloidin signal at the adipocyte cortex (500 adipocytes/section). Signal was measured in regions where neighboring adipocytes were in close association (see inset in A) to ensure only actin associated with the adipocyte membrane was measured. Data are expressed as fold changes from WT values ($n = 5$ mice/group). C) Representative western blots of total actin (C4 antibody) in WAT from WT (wt/wt), Tg (tg/tg) and KO (ko/ko) mice. D) Quantification of total actin blots corrected for total protein (Coomassie-stained gel). Data are expressed as fold change from WT values (set at 1) from $n = 4$ mice/group. E) Representative images of filamentous actin (F-actin) in WAT from WT and Tpm1.7 Tg mice visualized with phalloidin. Scale bars = 50 μM. F) Quantification of the phalloidin signal at the adipocyte cortex as in (B). Data are expressed as fold changes from WT values ($n = 3$/group). Data are mean ± SEM. Statistical differences are indicated by *$p < 0.05$ and +$p < 0.01$ (Kruskal–Wallis and Dunn multiple comparison tests).

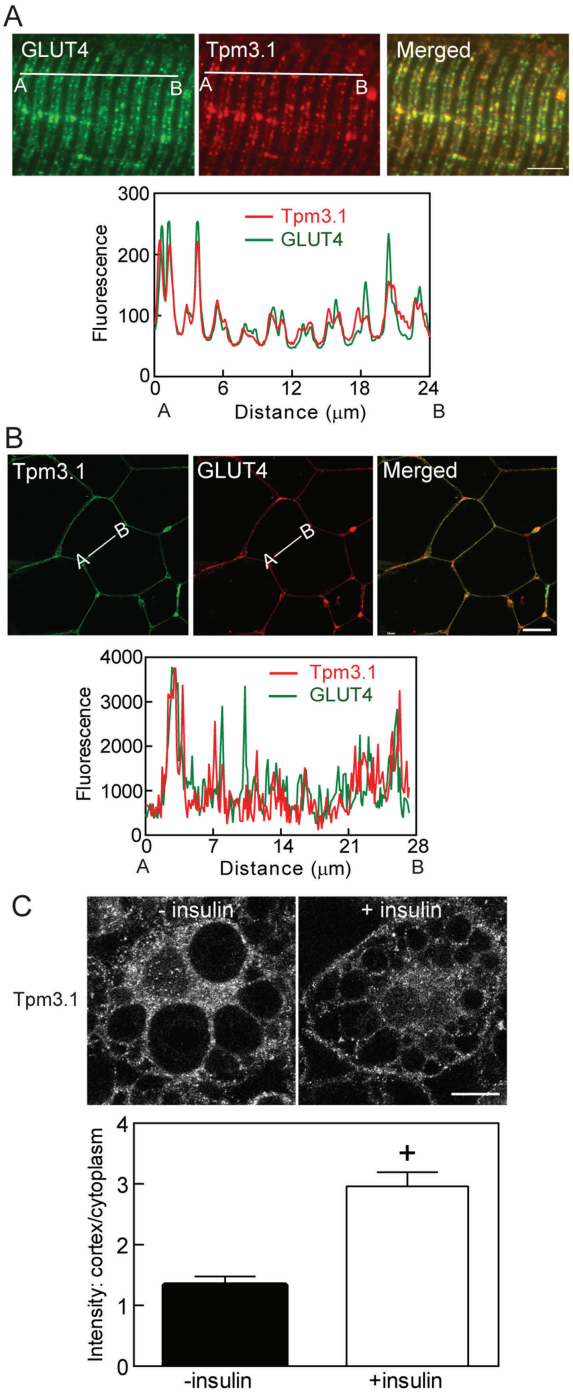

Figure 5: Legend on the next column.

with Tpm3.1 in the cell interior (Figure 7A, upper insert) and at the cell periphery (Figure 7A, lower insert) in differentiated adipocytes. Similar to Tpm3.1, MyoIIA accumulated at the cell cortex with insulin stimulation (Figure 7A) and also with TR100 treatment (Figure 7B). Myo1c is known to be involving in tethering GLUT4 vesicles via the exocyst complex to the PM (5,9). Interestingly, Myo1c was not localized with Tpm3.1 (Figure S4A) and Myo1c localization was unaffected by TR100 treatment (Figure S4B). TR100 also had no impact on the localization of Sec8 (Figure S4C), another component of exocyst complex. Collectively, these data indicate that Tpm3.1-containing actin filaments can selectively recruit myosin IIA motors to actin filaments in differentiated adipocytes.

Tpm3.1 regulates the levels of exocyst components

To determine if altered glucose uptake is due to impacts on specific pathways, we performed microarray gene expression profiling on WAT of Tg and WT mice. The complete list of significantly altered genes is available at the Gene Expression Omnibus (series record GSE25013). To determine which functional categories of genes were significantly affected by Tpm3.1, we performed functional annotation of the differentially expressed genes (>1.5-fold change) using Ingenuity Pathway Analysis (http://www.ingenuity.com). The Gene Ontology

Figure 5: Tpm3.1 colocalizes with GLUT4 in skeletal muscle and WAT, and is recruited to the plasma membrane with insulin stimulation in adipocytes. A) Upper panel: Representative immunofluorescent images of Tpm3.1 (γ/9d antibody) and GLUT4 in mouse skeletal muscle longitudinal sections. Both Tpm3.1 and GLUT4 are located in parallel striations consistent with T-tubule localization. Scale bar = 5 μm. Lower panel: Line scan across the muscle section showing significant colocalization of Tpm3.1 and GLUT4. B) Upper panel: Representative immunofluorescent image of Tpm3.1 and GLUT4 in mouse WAT showing Tpm3.1 and GLUT4 at the plasma membrane. Scale bar = 20 μm. Lower panel: Line scans across the WAT sections showing significant colocalization of Tpm3.1 and GLUT4. C) Upper panel: Representative immunofluorescent image of Tpm3.1 (γ/9d antibody) in differentiated 3T3-L1 adipocytes in the absence and presence of insulin showing an increase in cortical Tpm3.1 with insulin stimulation (100 nmol/mL for 30 min). Scale bars = 10 μm. Lower graph: Ratio of cortical-to-cytoplasmic Tpm3.1 signal in adipocytes showing a significant increase in Tpm3.1 at the cell cortex ($n = 10$ cells/group). Data are the mean ± SEM. Statistical significance is indicated by $+p < 0.01$ (Mann–Whitney *U* test).

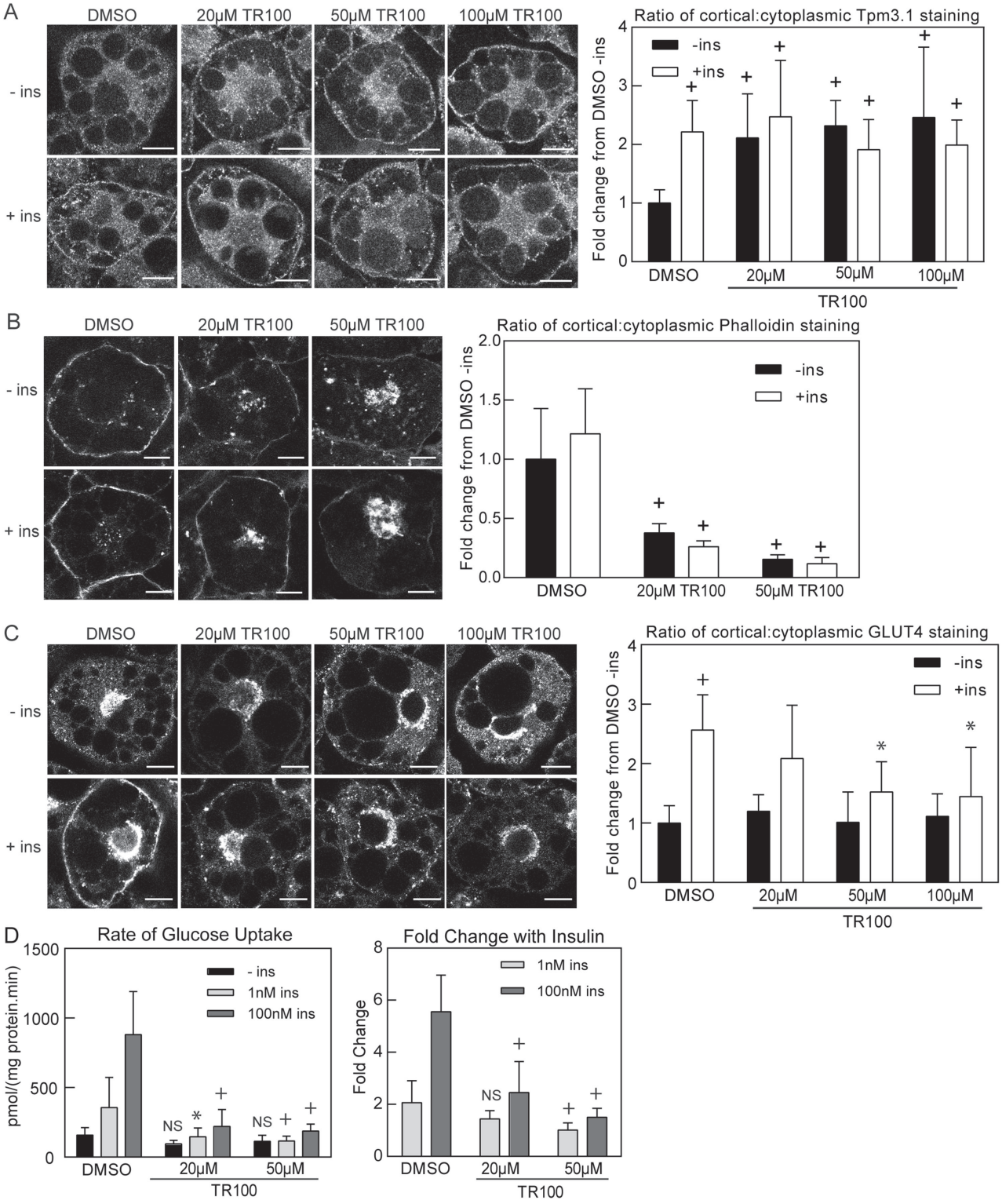

Figure 6: Legend on the next page.

categories significantly over-represented (enriched) in the differentially regulated genes were 'cellular metabolic', 'actin-filament-based, carbohydrate metabolic', 'glucose metabolic', 'regulation of transport' and 'exocytosis' (Table 1). The six genes in the 'exocytosis' class, *Myo1c*, *Exoc4* (Sec8), *Exoc2* (Sec5), *Myh9* (MyoIIA), *Stx4a* (Syntaxin 4) and *Stxbp4* (Synip) (Table 2), have all been implicated in GLUT4 exocytosis (42). Western blotting showed that the protein levels of two of these components, Sec8 and Myo1c, were significantly elevated in the WAT of the Tg mice (Figure 8A), whereas significant decreases were observed in the KO mice (Figure 8B). There were no significant changes in the levels of Syntaxin 4, the t-SNARE that mediates GLUT4 vesicle fusion with the PM, MyoIIA (data not shown) and GLUT4 in Tg and KO WAT (Figure 8A,B).

Tpm3.1 inhibits the interaction between actin and Myo1c

Changes in the levels of Tpm3.1-containing actin filaments and exocyst components are compatible with their involvement in transporting and/or tethering GLUT4 vesicle at the PM via Myo1c. We therefore tested the ability of Myo1c to power the motility of Tpm3.1-containing actin filaments using an *in vitro* motility assay (Figure 8C and Video S1). We found that higher surface densities of Myo1c were required to support *in vitro* actin gliding in the presence of Tpm3.1 (Figure 8C). Tpm3.1-inhibited actin filaments exhibited non-directional diffusional motion, indicating that Tpm3.1 inhibits the ability of Myo1c to enter into a force-generating state (Video S1). We conclude that while Tpm3.1-containing actin filaments can recruit MyoIIA (11 and Figure 7), they also function by restricting which actin filaments can bind Myo1c.

Discussion

Experiments in adipocyte and muscle cell culture systems have provided clear evidence for a role of the actin cytoskeleton in insulin-stimulated GLUT4 trafficking and glucose uptake (1–4,17,43–48). In these systems, insulin stimulates the remodeling of the cortical actin cytoskeleton (1,2,43,44,47) and inhibition of this remodeling with actin-destabilizing (Cytochalasin D or Latrunculin A/B) (1–4,17,43–46) or -stabilizing drugs (Jasplakinolide) (1,3) abrogates insulin-dependent GLUT4 vesicle fusion with the PM and glucose uptake. The role of the actin

Figure 6: Anti-Tpm3.1 compound TR100 inhibits insulin-stimulated GLUT4 trafficking and glucose uptake in 3T3-L1 adipocytes. A) Left: Representative immunofluorescent images showing impact of TR100 (1 h) on the localization of Tpm3.1 (γ/9d antibody) in differentiated 3T3-L1 adipocytes in the absence (−ins) and presence (+ins) of insulin (100 nmol/mL for 30 min). Scale bars = 10 μm. Right: Ratio of cortical-to-cytoplasmic Tpm3.1 signal in DMSO- (control) and TR100-treated cells with and without insulin ($n = 5$ cells/group; statistical significance is indicated by $+p < 0.01$ compared with DMSO/no insulin-treated cells, Kruskal–Wallis and Dunn multiple comparison tests). In control cells insulin treatment leads to a significant increase in Tpm3.1 at the cell cortex. TR100 treatment also leads to an increase in Tpm3.1 at the cell cortex. Insulin has no further impact. B) Left: Representative immunofluorescent images showing impact of TR100 (1 h) on the localization of filamentous actin (Phalloidin staining) in differentiated 3T3-L1 adipocytes in the absence (−ins) and presence (+ins) of insulin (100 nmol/mL for 30 min). Scale bars = 10 μm. Right: Ratio of cortical-to-cytoplasmic phalloidin (F-actin) signal in DMSO- (control) and TR100-treated cells with and without insulin ($n = 5$ cells/group; statistical significance is indicated by $+p < 0.01$ compared with DMSO/no insulin-treated cells, Kruskal–Wallis and Dunn multiple comparison tests). TR100 treatment leads to a dose-dependent decrease in F-actin at the cell cortex. Insulin had no further impact. C) Left: Representative immunofluorescent images showing impact of TR100 (1 h) on insulin-stimulated (100 nmol/mL for 30 min) increase in GLUT4 signal at the cell cortex in differentiated 3T3-L1 adipocytes. Scale bars = 10 μm. Right: Ratio of cortical-to-cytoplasmic GLUT4 signal in DMSO- (control) and TR100-treated cells with and without insulin ($n = 5$ cells/group; $+p < 0.01$ compared with no insulin at the same TR100 dose and $*p < 0.05$ compared with DMSO-treated cells, Kruskal–Wallis and Dunn multiple comparison tests). In control cells insulin treatment leads to a significant increase in GLUT4 at the cell cortex. TR100 treatment alone had no significant impact on GLUT4 at the cell cortex and prevented the insulin-stimulated movement of GLUT4 to the cell cortex. D) Insulin-stimulated glucose uptake is inhibited by TR100 (1 h) ($n = 3$ independent experiments). Statistical comparisons are shown versus DMSO-treated cells at the same insulin concentration: $*p < 0.05$; $+p < 0.01$; NS = not significant, $p > 0.05$ (Kruskal–Wallis and Dunn multiple comparison test). Data are mean ± SEM.

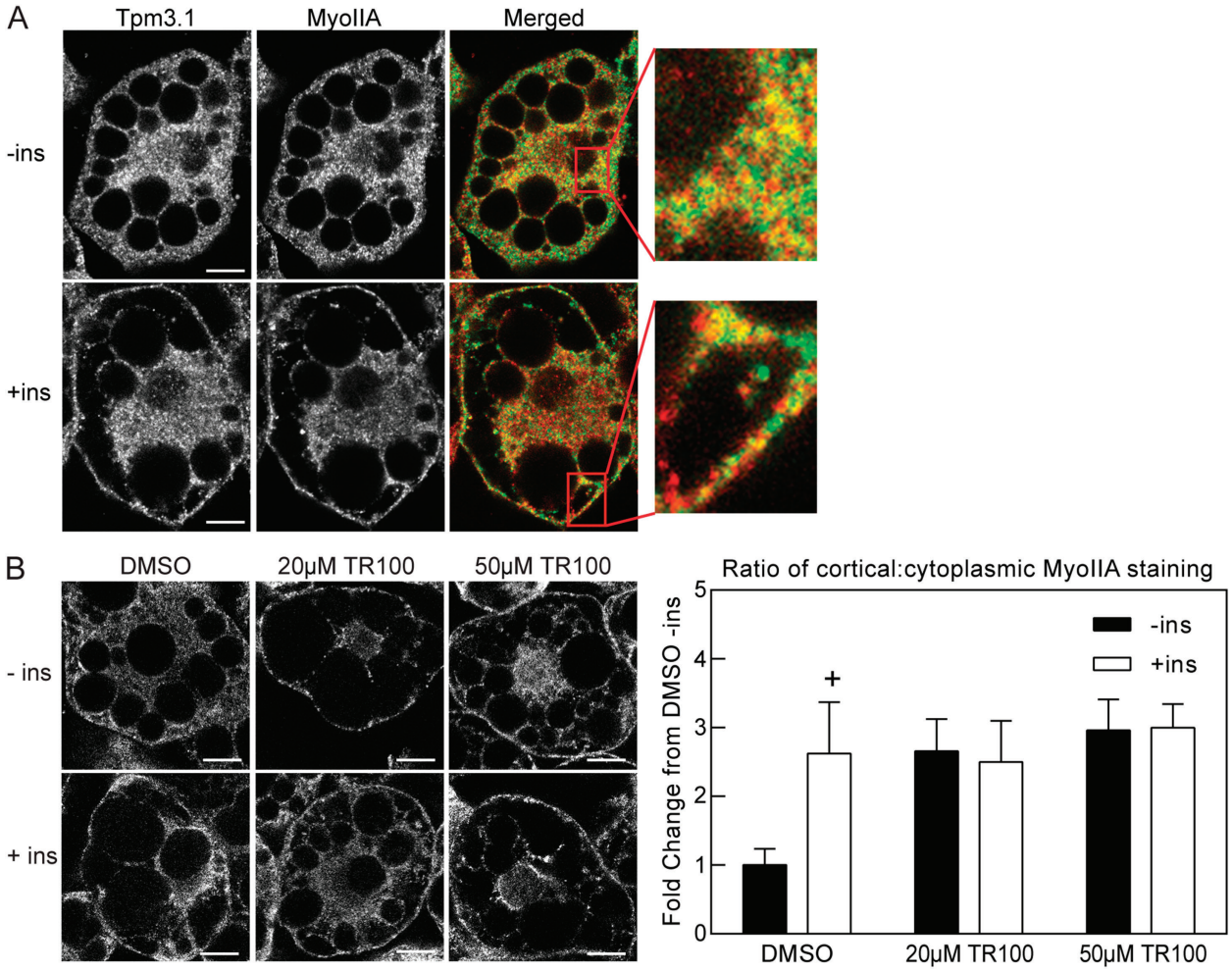

Figure 7: Tpm3.1 colocalizes with MyoIIA and the anti-Tpm3.1 compound TR100 disrupts insulin-stimulated movement of MyoIIA to the cell cortex in 3T3-L1 adipocytes. A) Representative immunofluorescent images of Tpm3.1 and MyoIIA in differentiated 3T3-L1 adipocytes in the absence (−ins) and presence (+ins) of insulin (100 nmol/mL for 30 min). Scale bars = 10 μm. In the basal and insulin-stimulated state there were areas of colocalization between Tpm3.1 and MyoIIA in the cell interior and at the cell cortex (see enlarged merged images); Pearson's correlation coefficient = 0.71 (−ins) and 0.67 (+ins). B) Left: Representative immunofluorescent images showing the impact of TR100 (1 h) on MyoIIA localization at the cell cortex in differentiated 3T3-L1 adipocytes in the absence (−ins) and presence (+ins) of insulin (100 nmol/mL for 30 min). Scale bars = 10 μm. Right: Ratio of cortical-to-cytoplasmic MyoIIA signal in DMSO- (control) and TR100-treated cells with and without insulin ($n = 5$ cells/group; statistical significance is indicated by +$p < 0.01$ compared with DMSO/no insulin-treated cell). In control cells (DMSO-treated), insulin treatment leads to a significant increase in MyoIIA at the cell cortex. TR100 treatment also produced a significant increase in MyoIIA at the cell cortex; insulin has no further impact. Data are mean ± SEM.

cytoskeleton in glucose uptake *in vivo* in animals has been more difficult to demonstrate in part due to the difficulty of targeting actin in the whole animal.

We have taken a different approach to understand the function of the actin cytoskeleton by targeting a core component of the actin filament, the tropomyosins. Tpms bind along the length of the actin filament and in an isoform-specific manner control the binding of myosin motors and actin-severing and actin-branching/nucleating proteins (12). This 'gatekeeper' function (49) of Tpms on the actin filament provides the means to create

Table 1: Gene ontology analysis (Ingenuity Pathway Analysis) of differentially expressed genes (>1.5-fold change) from Tpm3.1 Tg white adipose tissue

Biological process	No. genes increased in Tg mice	p-Value
Cellular metabolic	463	3.6×10^{4}
Actin filament-based	26	0.0019
Carbohydrate metabolic	48	0.0061
Glucose metabolic	17	0.029
Regulation of transport	29	0.030
Exocytosis	6	0.033

Table 2: Exocytosis genes increased in Tpm3.1 Tg white adipose tissue detected by Illumina gene expression array analysis

Gene	Fold change	p-Value
Myo1c	1.60	0.028
Exoc4 (Sec8)	1.53	0.023
Exoc2 (Sec5)	1.55	0.032
Myh9 (MyoIIA)	1.52	0.012
Stx4a (Syntaxin 4)	1.51	0.017
Stxbp4 (Synip)	1.51	0.021

structurally and functionally distinct actin filament populations based on Tpm isoform composition (12). Previously, we identified a γ-actin filament population in skeletal muscle defined by the tropomyosin Tpm3.1 that is distinct from the actin filament of the sarcomere and is located at the plasma and T-tubule membranes, sites of glucose uptake in skeletal muscle (15,33). In this study, we demonstrate that this Tpm isoform regulates insulin-stimulated glucose uptake. Overexpression of Tpm3.1 in a Tg mouse increased glucose clearance and insulin-stimulated glucose uptake in skeletal muscle, WAT and heart. This effect is Tpm3.1 dose-dependent and specific to Tpm3.1 as glucose clearance is unchanged in a mouse that expresses an unrelated Tpm isoform, Tpm1.7. Loss of Tpm3.1 leads to increased sensitivity to the detrimental effects of high fat feeding on glucose clearance.

The poorer clearance of the Tpm3.1 KO mice on HFD is an important finding as it implicates the actin cytoskeleton in the development of insulin-resistant states. This agrees with a number of previous studies that have shown that chronic insulin or high-glucose treatment to 3T3-L1 adipocytes and L6 myotubes leads to depleted cortical F-actin abundance and decreased insulin-dependent glucose transport (1,3,50). Furthermore, HFD fed insulin-resistant mice show reduced F-actin in skeletal muscle compared with normal chow-fed mice (51). Here we show that normally fed Tpm3.1 KO mice have decreased F-actin levels (Figure 4) but no change to glucose clearance (Figure S1). The HFD may have further depleted F-actin to a level that significantly impacted on glucose uptake.

Our data indicate that Tpm3.1 regulates glucose uptake via at least one step in GLUT4 trafficking. Firstly, Tpm3.1 is localized with GLUT4 in WAT and skeletal muscle. In 3T3-L1 adipocytes, there is increased translocation of Tpm3.1 from the cell interior toward the cell cortex in response to insulin consistent with involvement in GLUT4 exocytosis. However, the most direct demonstration of a role for Tpm3.1 in GLUT4 trafficking is the dramatic decrease in insulin-stimulated GLUT4 translocation to the cell surface and glucose uptake with the Tpm3.1 inhibitor, TR100. Importantly, TR100 has no effect on basal glucose uptake or basal GLUT4 localization, indicating that the drug has no general toxic effect on the cells and that its impact is specific to insulin-stimulated events.

TR100 is predicted to interact with the C-terminus of Tpm3.1 and has been shown to inhibit the actin filament-stabilizing action of Tpm3.1, leading to instability of Tpm3.1-containing actin filaments (41). Thus, the inhibition of GLUT4 translocation and glucose uptake by TR100 is consistent with a requirement for stable Tpm3.1-containing actin filaments in GLUT4 trafficking and glucose uptake. This is supported by: (i) the data in the Tg mice where an increase in Tpm3.1-containing filamentous actin in WAT is associated with an increase in glucose uptake and (ii) the data in 3T3-L1 adipocytes where the anti-Tpm3.1 drug results in reduction in the cortical actin cytoskeleton and abrogation of insulin-stimulated glucose uptake. In addition, it has recently been demonstrated that insulin-induced GLUT4 exocytosis is accompanied by capping of Tpm3.1-containing actin filaments by Akt2-dependent phosphorylation of tropomodulin 3 which promotes actin filament stability (52). Coupled with other studies showing that actin destabilization abrogates glucose uptake and GLUT4 trafficking events (1,2,4,8,43–46,53), our data support a model in which actin filament stabilization by Tpm3.1 is important in this process.

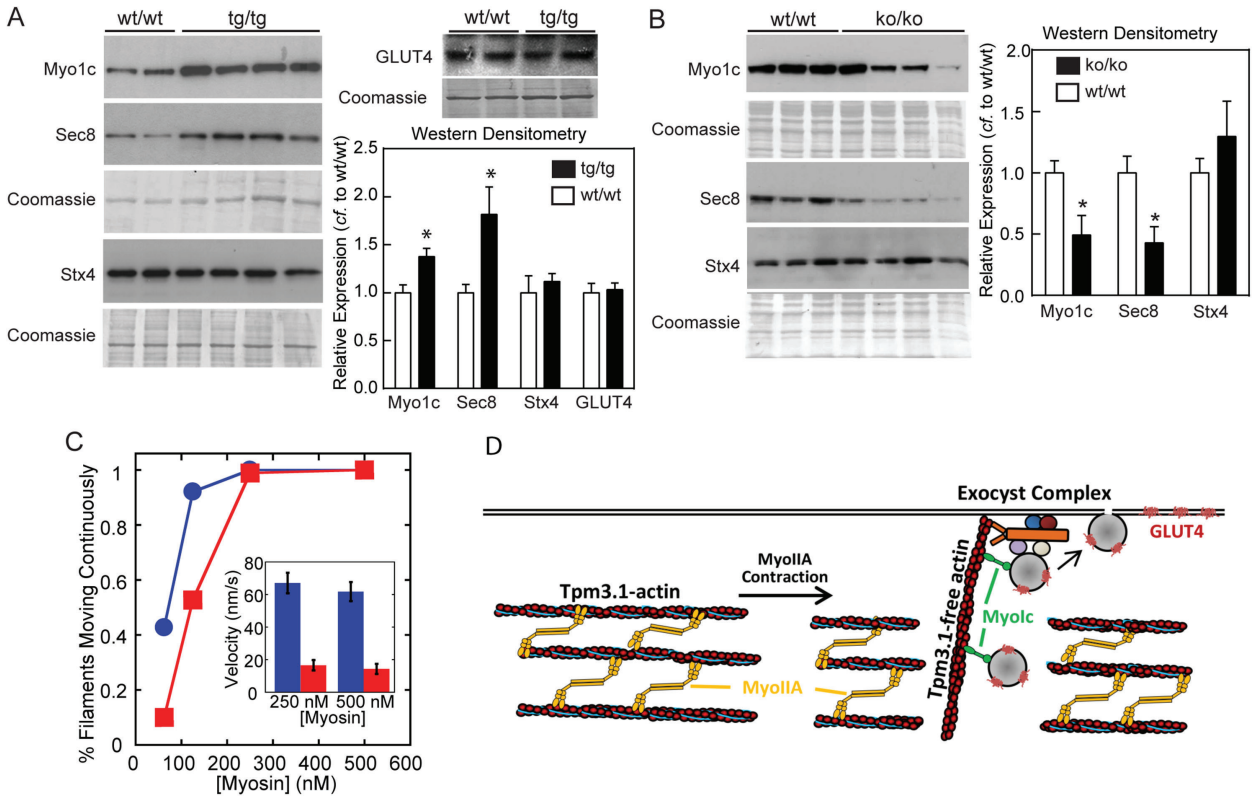

Figure 8: Tpm3.1 regulates levels of exocyst complex components and Myo1c activity. Representative western blots (left panels) and densitometric quantitation (right panels) of Myo1c, Sec8, syntaxin 4 (Stx4) and GLUT4 levels in WAT from WT (wt/wt), (A) Tpm3.1 Tg (tg/tg) and (B) KO (ko/ko) mice ($n = 6–8$/group; statistical significance is indicated by: *$p < 0.05$, Mann–Whitney *U* test). There was a statistically significant increase in Myo1c and Sec8 levels in Tg WAT compared with WT, while in KO WAT there a significant decrease. There was no significant difference in syntaxin 4 and GLUT4 levels in WAT from Tg or KO mice. C) Tpm inhibits Myo1c-driven actin gliding in an *in vitro* motility assay. The percentage of moving actin filaments that moved in a continuous, directional manner was measured as a function of Myo1c concentration as described in *Materials and Methods*. At [Myo1c] < 250 nM, the fraction of moving filaments was lower for Tpm-decorated actin (red) than for undecorated actin (blue). (Inset) The velocity of Myo1c-driven actin filament gliding at saturating [Myo1c] is slower for tropomyosin-decorated filaments. D) Schematic model of how the balance between Tpm3.1/MyoIIA and Tpm3.1-free/Myo1c actin filament populations may determine the efficiency of movement and/or fusion of GLUT4 vesicles with the plasma membrane. Data are mean ± SEM.

Altering Tpm expression alters actin filament dynamics. Tpm1.7 (Tm3) promotes the formation of short dynamic actin filaments (54), whereas elevated levels of Tpm4.2 (Tm4), enriched in the adhesion structures of osteoclasts (podosomes and sealing zones), result in thickening of these structures owing to an increase in F-actin (55). Similarly, we found in primary cortical neurons and B35 neuroblastoma cells that an elevated level of Tpm3.1 promotes stress fiber formation and enhances tension-conferring myosin II activation and recruitment to stress fibers (11,18,34). Here we show that Tpm3.1 colocalizes with MyoIIA in 3T3-L1 adipocytes and inhibition of Tpm3.1 function (with TR100) disrupts MyoIIA localization. In addition, Tpm3.1 has been shown to promote the stabilization of focal adhesions (56). Tpm3.1 is thought to stabilize actin filaments by inhibiting the interaction of actin-depolymerizing factors such as ADF/cofilin and gelsolin with actin (11,19–21) and promoting the recruitment of tropomodulins (Tmods) to the 'pointed' ends of actin filaments inhibiting pointed-end actin filament turnover (57). In this regard, data in adipocytes (52) and in skeletal muscle (58) indicate that Tmod3

preferentially associates with Tpm3.1-containing actin filaments. Here we report that Tpm *in vivo* is limiting for the formation of filamentous actin in adipocytes, independent of the Tpm isoform. Remarkably, in the absence of Tpm3.1 there is a decrease in the levels of F-actin in adipocytes indicating that Tpm3.1 is required to maintain the pool of filamentous actin. This provides *in vivo* support for a model where increased levels of Tpm bind to and stabilize populations of Tpm-free F-actin and also drive actin polymerization toward increased filamentous actin (34). Thus, altered levels of Tpm3.1 are expected to lead to altered levels of Tpm3.1-containing actin filaments and by association, altered levels of Tpm-free actin filaments.

There has been debate about the specific role of the actin cytoskeleton in GLUT4 trafficking (59,60). It has been suggested that actin functions as a 'track' for movement of GLUT4-containing vesicles from intracellular sites to the membrane or provides force for the later stage of fusion of vesicles with the PM. However, there is increasing evidence for a role of the actin cytoskeleton in the more distal steps of the GLUT4 trafficking pathway, particularly the tethering or docking of GLUT4 vesicles with the surface membranes (48,60). A key finding is that the actin-monomer sequestering drug Latrunculin B inhibits GLUT4 vesicle fusion, but not the movement of vesicles to the cortical region (4), suggesting that the formation of new actin filaments is crucial for either tethering and/or fusion of GLUT4 vesicles with the surface membranes. More recently, Boguslavsky et al. (5) showed that insulin reduces the mobility of GLUT4 vesicles at the sub-membrane region and that this immobilization is mediated by tethering of the vesicles to the cortical actin filament network via Myo1c.

Our data also show that the interaction between Myo1c and actin is inhibited by Tpm3.1. It is possible that the distribution between Tpm3.1-containing and Tpm3.1-free actin filaments may determine the efficiency of movement of GLUT4 through the cortical actin mesh to the membrane. This is consistent with the recent observation that the presence of Tpm1.6 (Tm2) on an actin filament makes these filaments inaccessible to Myo1c (61). Limiting the number of Myo1c-permissive filaments would be expected to make movement of Myo1c-containing filaments more coherent in the presence of a high density of non-competing Tpm3.1-containing filaments. Conversely, the high density of Tpm3.1-containing filaments would be expected to promote engagement with MyoIIA motors (11) and the generation of cortical contractile force which may promote vesicle penetrance of the cortical mesh (see model, Figure 8D). It has recently been shown that recruitment of MyoIIA to the cortical actin filaments in adipocytes is required for GLUT4-mediated glucose uptake (62). Thus, the amount of Tpm3.1 may determine the amount of contractile force that can be generated by cortical actin filaments. It is also worth noting that our data show that Tpm1.7 can regulate the quantity of actin filaments, containing Tpm1.7, but does not impact glucose transport. This suggests that the interaction between MyoIIA-, Myo1c- and Tpm1.7-decorated filaments may be different than the interaction with Tpm3.1 filaments. This is consistent with other studies showing that the regulation of different myosin isoforms is Tpm isoform-specific (25,29–31). Thus, the use of different Tpms and generation of Tpm-free actin filaments provide spatial and temporal specification of the qualitative and quantitative properties of actin filament function depending on both the availability and quantity of specific Tpm isoforms (12).

Materials and Methods

Antibodies and anti-Tpm compound

Tpm isoform-specific Tpm antibodies are described by Schevzov et al. (63): γ9d (sheep polyclonal and mouse monoclonal antibodies) recognizes the 9d exon from the *Tpm3* gene (both human and mouse) corresponding to Tpm3.1 (Tm5NM1) and Tpm3.2 (Tm5NM2); CG3 (mouse monoclonal antibody) recognizes the 1b exon from the *Tpm3* gene, which is contained in all cytoskeletal (non-muscle) Tpms (64). Primary antibodies used: Akt and phospho-Akt (Ser473) rabbit polyclonals (1:1000; Cell Signalling Technology, Inc.); GLUT4 (1F8) mouse monoclonal (1:3000 for western blots; 1:200 for immunofluorescence staining) (from David James) (65); rSec8 mouse monoclonal (Stressgen); Myo1c (M2) mouse monoclonal (66); syntaxin 4 rabbit polyclonal (Synaptic Systems); α-tubulin mouse monoclonal (DM1a) (Sigma) and MyoIIA rabbit polyclonal (Covance). Secondary antibodies used for western blot analysis: anti-rabbit, anti-sheep and anti-mouse IgG-conjugated horseradish peroxidise (HRP) (GE Healthcare) and donkey/anti-rabbit/HRP antibodies (for Akt western blots) (Jackson ImmunoResearch Laboratories).

The anti-Tpm compound TR100 has been designed to target Tpm3.1 using the sequence divergence at the C-terminus of cytoskeletal versus muscle Tpms. This compound targets Tpm3.1 and disrupts actin filaments by inhibiting the actin filament-stabilizing action of Tpm3.1 (41).

Mice

Animal experiments were performed in accordance with the UNSW Australia Animal Care and Ethics Committee and the Australian National Health and Medical Research Council 'Code' and guidelines. The Tpm3.1 (Tm5NM1) Tg and the Tpm3.1 KO [B6-*Tpm3*$^{tm2(\Delta 9d)Pgun}$] mouse lines were described by Bryce et al. (11) and Vlahovich et al. (15), respectively. The Tpm3.1 Tg mice express the human form of Tpm3.1 under the control of the human β-actin promoter and therefore the transgene is expressed in all tissues. We have generated Tpm3.1 Tg mice on two different backgrounds, FVB/N [F-Tg(*ACTB-TPM3.Tm5NM1*)Pgun] and C57BL/6 [B6.F-Tg(*ACTB-TPM3.Tm5NM1*)52 Pgun]. The FVB/N Tg line is the original line (11) and has been maintained on a FVB/N background for >10 generations. The Tg mice on the C57BL/6 background were generated from the FVB/N line by speed congenic backcrossing (at six generations mice were 99.9% congenic by SNP analysis) (Transgenic Services of Queensland, St Lucia, QLD, Australia). In the Tpm3.1 KO mice exon 9d from the *Tpm3* gene, coding for Tpm3.1, is absent. These mice have been maintained on a C57BL/6 background for >10 generations. All mice were maintained in a temperature-controlled facility (22–24°C) on a 12-h (light 0700 h; dark 1900 h) cycle. Chow-fed mice received a normal chow diet (Rat Maintenance Diet, Gordon's Specialty Feeds) containing 8% fat, 21% protein and 71% carbohydrate (as calories) plus fiber, vitamins and minerals. High fat-fed mice received a custom-made HFD composed of 45% calories as fat, 20% protein and 35% carbohydrate made in-house as described by Turner et al. (67). WT control mice for homozygous lines were age-matched mice of the same background strain bred in the same facility. For heterozygous Tg mice, WT littermate controls were used. Only male mice were used in this study.

Western blotting

For Tpm western blots, tissue was extracted in ice-cold extraction buffer (50 mM Tris-Cl, pH 7.5) and solubilized using a sonicator as described by Schevzov et al. (68). For all other western blots, protein was extracted in radioimmunoprecipitation assay buffer (RIPA) [20 mM Tris pH 7.4, 150 mM sodium chloride, 1% Nonidet P-40, 0.5% sodium deoxycholate, 1 mM EDTA, 0.1% SDS, protease inhibitor tablet (Complete Mini Protease Inhibitor EDTA free tablet; Roche Diagnostics Corporation) and phosphatase inhibitor cocktail tablet (PhosSTOP; Roche Diagnostics Corporation)]. Epididymal WAT, whole heart and tibialis anterior muscles were used for WAT, heart and skeletal muscle samples, respectively. The samples were homogenized in a volume of 20 times tissue weight with a plastic pestle and incubated for 20 min on ice. The insoluble matter was removed by centrifuging at 15 000× ***g*** at 4°C for 10 min. Protein concentration was determined using a BCA Protein Detection Kit (Pierce) and extracts were solubilized in SDS buffer (68).

SDS–PAGE (12.5 or 7.5%) and western blotting were performed as described by Schevzov et al. (68). Protein was transferred onto PVDF membranes (Millipore) and blocked in either 5% skim milk or 1% BSA in TTBS (100 mM Tris–HCl pH 7.5, 150 mM NaCl and 0.1% Tween 20) for 1–2 h. Blots were incubated (2 h, room temperature or 4°C, overnight) with primary antibodies diluted in TTBS (CG3, 1:100; γ9d, 1:500) or 1% BSA/TTBS (Akt, 1:1000; P-Akt, 1:1000; Sec8, 1:1000; Myo1c, 1:1000; Syntaxin 4, 1:2000). Blots were then incubated (1 h at room temperature) with HRP-labeled secondary antibodies (1:10 000 dilution) in either TTBS, for anti-Tpm antibodies, or 2% skim milk/TTBS for other antibodies, and then washed with TTBS (4 x 15 min). Antibody binding was detected by Western Lighting Chemiluminescence Reagent (PerkinElmer Life Sciences) and exposed to Fuji X-ray Film (Kodak). For the quantification of western blots, X-ray films were scanned and densitometry performed using the Molecular Imager Chemi-doc XRS and integrated software (Bio-Rad).

Glucose and insulin tolerance tests

GTT and ITT were performed in 14–16 h fasted mice as previously described (69). Sterile glucose [2 g/kg body weight (BW)] or insulin (0.5 or 1.5 U/kg BW for normal and high-fat fed mice, respectively; Actrapid, Novo Nordisk) was injected (i.p.) into mice and blood samples were obtained from the tail tip at the indicated times. Glucose levels were measured using a glucometer (AccuCheck Performa; Roche Diagnostics).

In vivo glucose uptake during a glucose tolerance test

Measurement of glucose uptake into tissues is based on Cooney et al. (70) and Zisman et al. (71). A sterile glucose solution (2 g/kg BW) containing 2-deoxy-D-[1,2-^{3}H]-glucose (2-DOG; 370 kBq/mouse) (Perkin Elmer) was injected intraperitoneally into mice. Blood samples (20 μL) were taken from tail veins at 0, 15, 30, 45, 90 and 120 min post-injection and blood glucose concentrations were measured using a glucometer (AccuCHEK Performa). At 120 min post-injection, tissues were rapidly frozen in liquid nitrogen for analysis of 2-DOG uptake.

To determine glucose-specific radioactivity (SRA) in blood, 3 μL of plasma was deproteinized with 200 μL of 3.5% ice-cold perchloric acid, centrifuged and the supernatant neutralized with 45 μL 2.2 M $KHCO_3$. Radioactivity was then measured in a scintillation counter (Perkin Elmer, Tricarb 2800TR). The plasma-glucose SRA (disintegrations/min/μmol) was calculated by dividing plasma radioactivity-AUC by glucose AUC over the 120 min of the experiment. 2-DOG is transported into tissues and phosphorylated, but does not enter glycolysis (72). To determine tissue accumulation of 2-DOG-6-phosphate, 100–200 mg of tissue was homogenized in 2 mL of distilled water, and 1.6 mL of the homogenate was deproteinized with 1.6 mL of 7% ice-cold perchloric acid. The precipitated protein was removed by centrifugation, and 2.5 mL of the supernatant was neutralized for 30 min with 625 μL of 2.2 M $KHCO_3$. The resulting precipitate was removed by centrifugation and the supernatant was divided into two 800 μL aliquots. Total radioactivity was measured on one aliquot and the other aliquot was passed through an AG 1-X8 anion exchange column (Bio-Rad) to remove 2-DOG-6-phosphate. The column was washed three times with 3 mL of distilled water and the radioactivity of the eluate was determined in a scintillation counter. The difference between total and eluted ^{3}H radioactivity represents the amount of accumulated 2-deoxy-D-[1,2-^{3}H]-glucose-phosphate in the tissue. To calculate 2-DOG uptake by the tissue, the tissue ^{3}H-2-DOG-6-phosphate radioactivity (disintegrations/minute) was divided by the integrated

plasma-glucose-specific activity under the curve and the quantity of tissue extracted.

Food intake, activity and indirect calorimetry

Ad libitum food intake, activity and indirect calorimetry were measured using the metabolic cage system (CLAMS) from Columbus Instruments as described (73). Measurements were begun at 1600 h. The first of the measurement periods (24 h) was an acclimatization period and the last 24 h (0700–1900 h) was used for analysis. Activity (number of beam breaks) was recorded continuously in the *X* and *Z* directions. The calorimeter was calibrated before experiment with a standard span gas (0.50% CO_2, 20.4% O_2 balanced with N_2) and cross calibrated with room air.

Immunohistochemistry

Mouse soleus muscle were fixed in 4% paraformaldehyde (PFA) (hindlimb muscles were stretched and held during fixation) and infused with 1.8 M sucrose/20% polyvinylpyrrolidone as described by Vlahovich et al. (74). Semi-thin (0.5–0.8 µm) sections were cut at −60°C using an Ultracut UCT ultramicrotome (Leica) equipped with an EM FCS cryochamber (Leica). WAT was fixed in 10% buffered formalin and embedded in paraffin. 3T3-L1 adipocytes were fixed in 4% PFA at room temperature for 15 min and permeabilized and blocked (2% BSA and 0.1% saponin in PBS) at room temperature for 30 min.

Adipocytes on cover slips were blocked in 3% BSA in PBS overnight and incubated (1 h, room temperature) with primary antibodies diluted in PBS (GLUT4 and γ9d, both at 1:200 dilution) and then with Alexa-488-conjugated goat anti-mouse and Alexa-555-conjugated goat anti-rabbit secondary antibodies (1:500 dilution) in PBS (1 h, room temperature). Sections were washed three times with PBS and mounted with Immuno-Mount (Thermo Fisher Scientific). Filamentous actin was visualized in WAT sections using phalloidin (34).

Microscopy and image analysis

Microscopy and imaging were performed using a Leica TCS SP5 (Leica) confocal microscope with 63x NA1.4 objective. To quantify the intensity of cortical staining in adipocytes five separate line scans were performed for each cell using ImageJ software, and the maximum fluorescence intensity at the cell cortex corrected for intensity of the cell cytoplasm was obtained. This was performed on 5–10 different cells for each treatment condition to obtain the mean fluorescence intensity. The extent of colocalization of two proteins was determined using ImageJ colocalization analysis plug-in (75). Results are presented as Pearson correlation coefficients, which represent the linear relationship of the signal intensity from the green and red channels of the analyzed image. At least 20 cells were analyzed for each condition.

Cell culture

The 3T3-L1 cells (passages 8 and 11) were obtained from David James (Garvan Institute, Sydney, NSW) who originally obtained the cells from Howard Green (Harvard University). 3T3-L1 fibroblasts were cultured in DMEM/high glucose supplemented with 10% (v/v) FBS, 50 mg/L penicillin and 50 mg/L streptomycin. Cells were maintained in a humidified atmosphere with 5% CO_2 at 37°C. To maintain the proliferative potential of the cells, cultures were split three times per week and cells used only up to passage 21. For microscopy and imaging experiments, 3T3-L1 adipocytes were cultured and differentiated as described by Larance et al. (76). Fully differentiated cells (8 days of differentiation) were treated with TR100 or vehicle (DMSO) for 1 h and fixed.

Insulin-stimulated glucose uptake in adipocytes

Insulin-stimulated glucose uptake was performed essentially as described by Shi and Kandror (77). 3T3-L1 cells were grown and differentiated in 12-well plates and glucose uptake experiments were performed between days 8 and 10 of differentiation. 3T3-L1 adipocytes were incubated in serum-free DMEM for 1 h at 37°C and then with serum-free DMEM containing DMSO (control) or TR100 (20, 50 and 100 µM) for another hour at 37°C. The cells were then incubated with 1 or 100 nM insulin at 37°C for 15 min in 450 µL KRP buffer (120 mM NaCl, 0.6 mM Na_2HPO_4, 0.4 mM NaH_2PO_4, 6 mM KCl, 1.2 mM $MgSO_4$, 12.5 mM HEPES, 1 mM $CaCl_2$ and 0.2% (w/v) BSA, pH7.4). Glucose transport was initiated by the addition of 50 µL KRP buffer containing 0.5 mM ^{3}H-2-deoxy-D-glucose (18.5 kBq) to each well. After 5 min, the reaction was terminated by washing with ice-cold PBS three times. Cells were solubilized with 250 µL of 1% Triton in PBS, and 200 µL of the lysates was taken to determine incorporated radioactivity by liquid scintillation counting. Each experimental condition was analyzed in triplicate.

Illumina BeadArray analysis

Gene expression profiling was performed on epididymal adipose tissue from Tpm3.1 Tg (tg/tg) and WT control mice (14–16 h fasted, 4 months old, male mice; $n = 5$ and 4/group, respectively) using Illumina 46K mouse BeadArrays as outlined by Pearen et al. (78). RNA was extracted using TRI-Reagent (Sigma Aldrich) according to the manufacturer's directions. RNA was purified using a mini-RNeasy kit (QIAGEN) according to the kit instructions. Integrity of the total RNA samples was assessed using the Agilent Bioanalyzer 2100 and RNA integrity scores above 7.8 were present in all samples. Amplified cRNA (1500 ng) was hybridized to Sentrix Mouse-6.v1 BeadChip arrays (Illumina). BeadChip arrays were scanned with an Illumina BeadStation Scanner and the data imported into Gene-Spring GX v7.3.1 software (Agilent) for data analysis. Data were normalized to control genes, genes with an Illumina detection score equal to one, and all probes except the genes with an Illumina detection score equal to one were filtered out to remove probes without adequate expression levels. A parametric Welsh's test (unequal variance) was performed (p-value cutoff = 0.05) and multiple testing correction (Benjamini and Hochberg False Discovery Rate) was then applied to genes that passed the Welch's test. Ingenuity Pathway Analysis (http://www.ingenuity.com) was performed on genes with positive fold changes between Tg and WT tissue of greater than 1.5 (1283 transcripts).

In vitro Myo1c motility assays

Constructs consisting of the motor domain and three IQ motifs of mouse MYO1C were expressed in *Sf*9 cells, and purified as described (79,80). Non-muscle actin (human platelet) was purchased from Cytoskeleton Inc. Human Tpm3.1 was expressed, purified and was reduced on the day of the experiment as previously described (41). *In vitro* motility assays were conducted as previously described with the following modifications (80,81). Experiments were performed at 37°C in KMg25 buffer (25 mM KCl, 60 mM MOPS pH 7.0, 1 mM $MgCl_2$, 1 mM EGTA and 1 m*m* DTT). For the experiments with Tpm-decorated actin, 40 nM rhodamine phalloidin actin was premixed with 5 μM Tpm3.1 and this mixture was added to the flow cell in the same manner as bare actin. Two micromolars of Tpm3.1 was included in the final activation buffer to ensure that the actin filaments remained decorated throughout the experiment. Sliding velocity was quantified via manual tracking using the ImageJ plugin MTrackJ (82) and error bars show the standard deviation. For the analysis of the percentage of filaments moving continuously, all filaments in the field of view were examined over several fields of view. At least 100 filaments were first classified as either moving or completely immotile. Filaments motion was then determined to be either continuous (i.e. moving directionally for at least six consecutive frames taken 10 seconds apart during the 2- to 5-min-long movie) or diffusive. Immotile filaments were not included in the analysis.

Statistical analysis

For all but the BeadArray data, statistical significance was tested (GraphPad Prism 6.01 software) at $p < 0.05$ levels using Student's *t*-test or the non-parametric Mann–Whitney *U* test for data that were not normally distributed (D'Agostino and Pearson normality test) or for datasets too small to assess normality. Data are expressed as mean ± SEM.

Acknowledgments

We thank Galina Schevzov for western blot analysis of muscle tissue, Nicole Vlahovich for skeletal muscle immunofluorescence analysis and the BioMedical Imaging Facility at UNSW under the direction of Renee Whan for help with the microscopy. This work was supported by Australian National and Medical Research Council (NHMRC) Grants 321705 (P. W. G., E. C. H. and A. J. K.) and 1026616 (P. W. G., E. C. H., A. J. K. and W. E. H.), Diabetes Australia (E. C. H., A. J. K. and P. W. G.) and funding from The Kids' Cancer Project (P. W. G., E. C. H. and A. J. K.), intramural funding from A*STAR (Agency for Science, Technology and Research) Biomedical Research Council (W. H.) and an NIH Grant (GM057247, M. J. G. and E. M. O). Peter Gunning is a Director on the Board of Novogen, a company which is commercializing drugs that are directed against the tropomyosin Tpm3.1 and that is used in this study.

Supporting Information

Additional Supporting Information may be found in the online version of this article:

Video S1: Myo1c-driven gliding assays. The rate of Myo1c-driven gliding of actin both in the presence and absence of Tpm3.1 was measured. As the concentration of Myo1c on the surface was reduced, motile filaments began to diffuse rather than move directionally, indicative of reduced binding of Myo1c to actin. This reduction in binding at [Myo1c] < 250 nM was greater in the presence of Tpm3.1, indicative of the fact that Tpm3.1 inhibits the interaction of Myo1c and actin.

Figure S1: Glucose tolerance tests (GTT), insulin tolerance tests (ITT), respiratory exchange ratios and activity of Tpm3.1 KO mice on normal and high-fat diet (HFD). (A) GTT and (B) area-under the curve (AUC) of the GTT for 12-week-old mice on normal chow showing no difference in Tpm3.1 KO mice ($n = 17–18$/group). (C) ITT (0.5 U/kg body weight) and (D) area-above the curve (AAC) of the ITT for 12-week-old mice on normal chow showing no difference in insulin sensitivity in KO mice ($n = 18$/group). (E) Daily (24 h) food intake in WT and KO mice on normal chow and 8 weeks of HFD ($n = 5–6$/group). There was no significant difference between WT and KO mice for food intake on the two diets. (F) Respiratory exchange ratio (RER) for WT and KO mice on normal chow and 8 weeks of HFD ($n = 5–6$/group). Shown are data for RER averaged over 24 h (light period 0700–1900 h; dark period 1900–0700 h). An RER of 0.70 indicates that fat is the predominant fuel source, RER of 0.85 suggests a mix of fat and carbohydrates and a value of 1.00 or above is indicative of carbohydrate being the predominant fuel source. There was no significant difference between WT and KO mice for RER in any time period on the two diets. (G) Ambulatory activity of WT and KO mice on normal chow and 8 weeks of HFD ($n = 5–6$/group). Shown are data for total activity averaged over 24 h (light period 0700–1900 h; dark period 1900–0700 h). There was no significant difference between WT and KO mice for activity at any time of day.

Figure S2: Metabolic data for Tpm3.1 Tg mice on the FVB/N background. (A) Glucose tolerance test (GTT) and (B) area-under-the-curve (AUC) of the GTT for 12-week-old mice on normal chow showing increased clearance in Tpm3.1 Tg (tg/tg, tg/wt) versus WT (wt/wt) mice ($n = 6–10$/group; statistical significance is indicated by $^*p < 0.05$, $^+p < 0.01$; Mann–Whitney *U* test). (C) Insulin tolerance test (ITT) and (D) area-above-the curve (AAC) of the ITT for 12-week-old mice on normal chow showing increased insulin sensitivity of the Tpm3.1 Tg mice ($n = 11–14$/group; statistical significance is indicated by $^*p < 0.05$; *t*-test). (E) Daily (24 h) food intake in 14-week-old WT and Tpm3.1 Tg mice ($n = 5–6$/group) showing no significant difference. (F) Respiratory exchange ratio (RER) for 14-week-old WT and Tpm3.1 Tg mice. Left: RER averaged over 24 h; Middle: RER averaged over the light period (0700–1900 h); Right: RER averaged over the dark period (1900–0700 h). An RER of 0.70 indicates that fat is the predominant fuel source, RER of 0.85 suggests a mix of fat and carbohydrates and a value of 1.00 or above is indicative of carbohydrate being the predominant fuel source. There was no significant difference between WT and Tg mice for RER at any time of day ($n = 5–6$/group). (G) Ambulatory activity for 14-week-old WT and Tpm3.1 Tg mice. Left: Activity averaged over 24 h; Middle: activity averaged over the light period (0700–1900 h); Right: activity averaged over the dark period (1900–0700 h) ($n = 5$ mice/group). There was no significant difference between WT and Tg mice for activity at any time of day.

Figure S3: Insulin-stimulated Akt phosphorylation in white adipose tissue (WAT) and skeletal muscle from Tpm3.1 Tg mice (FVB/N background). Western blots of Akt and phospho-Akt (Ser473) in (A) WAT

and (C) skeletal muscle with (+) and without (−) insulin injection (0.5 U/kg body weight, i.p.) in fasted (14–16 h), 10- to 11-week-old WT (wt/wt) and Tpm3.1 Tg (tg/tg) mice. Densitometric quantitation of Akt and phospho-Akt (Ser473) levels in (B) WAT and (D) skeletal muscle ($n = 3–4$ mice/group). There was no significant difference in the levels of total Akt or phospho-Akt (with or without insulin treatment) between WT and Tg mice in either tissue.

Figure S4: Impact of insulin and the anti-Tpm3.1 compound TR100 on Myo1c and Sec8 localization in differentiated 3T3-L1 adipocytes. (A) Representative immunofluorescent images of Tpm3.1 and Myo1c in differentiated 3T3-L1 adipocytes in the absence (−ins) and presence (+ins) of insulin (100 nmol/mL for 30 min). Scale bars = 10 μm. In the basal and insulin-stimulated state there was no colocalization between Tpm3.1 and MyoIc. (B) Representative immunofluorescent images showing impact of TR100 (1 h) on the localization of Myo1c in differentiated 3T3-L1 adipocytes in the absence (−ins) and presence (+ins) of insulin (100 nmol/mL for 30 min). Scale bars = 10 μm. TR100 had no impact on Myo1c localization. (C) Representative immunofluorescent images showing impact of TR100 (1 h) on the localization of Sec8 in differentiated 3T3-L1 adipocytes in the absence (−ins) and presence (+ins) of insulin (100 nmol/mL for 30 min). Scale bars = 10 μm. TR100 had no impact on Sec8 localization.

References

1. Kanzaki M, Pessin JE. Insulin-stimulated GLUT4 translocation in adipocytes is dependent upon cortical actin remodeling. J Biol Chem 2001;276:42436–42444.
2. Khayat ZA, Tong P, Yaworsky K, Bloch RJ, Klip A. Insulin-induced actin filament remodeling colocalizes actin with phosphatidylinositol 3-kinase and GLUT4 in L6 myotubes. J Cell Sci 2000;113:279–290.
3. Tong P, Khayat ZA, Huang C, Patel N, Ueyama A, Klip A. Insulin-induced cortical actin remodeling promotes GLUT4 insertion at muscle cell membrane ruffles. J Clin Invest 2001;108:371–381.
4. Lopez JA, Burchfield JG, Blair DH, Mele K, Ng Y, Vallotton P, James DE, Hughes WE. Identification of a distal GLUT4 trafficking event controlled by actin polymerisation. Mol Biol Cell 2009;20:3918–3929.
5. Boguslavsky S, Chiu T, Foley KP, Osorio-Fuentealba C, Antonescu CN, Bayer KU, Bilan PJ, Klip A. Myo1c binding to submembrane actin mediates insulin-induced tethering of GLUT4 vesicles. Mol Biol Cell 2012;23:4065–4078.
6. Bose A, Robida S, Furcinitti PS, Chawla A, Fogarty K, Corvera S, Czech MP. Unconventional myosin Myo1c promotes membrane fusion in a regulated exocytic pathway. Mol Cell Biol 2004;24:5447–5458.
7. Toyoda T, An D, Witczak CA, Koh HJ, Hirshman MF, Fujii N, Goodyear LJ. Myo1c regulates glucose uptake in mouse skeletal muscle. J Biol Chem 2011;286:4133–4140.
8. Hagan GN, Lin Y, Magnuson MA, Avruch J, Czech MP. A rictor-Myo1c complex participates in dynamic cortical actin events in 3T3-L1 adipocytes. Mol Cell Biol 2008;28:4215–4226.
9. Chen XW, Leto D, Chiang SH, Wang Q, Saltiel AR. Activation of RalA is required for insulin-stimulated Glut4 trafficking to the plasma membrane via the exocyst and the motor protein Myo1c. Dev Cell 2007;13:391–404.
10. Bose A, Guilherme A, Robida SI, Nicoloro SMC, Zhou QL, Jiang ZY, Pomerleau DP, Czech MP. Glucose transporter recycling in response to insulin is facilitated by myosin Myo1c. Nature 2002;420:821–824.
11. Bryce NS, Schevzov G, Ferguson V, Percival JM, Lin JJ, Matsumura F, Bamburg JR, Jeffrey PL, Hardeman EC, Gunning P, Weinberger RP. Specification of actin filament function and molecular composition by tropomyosin isoforms. Mol Biol Cell 2003;14:1002–1016.
12. Gunning P, O'Neill G, Hardeman E. Tropomyosin-based regulation of the actin cytoskeleton in time and space. Physiol Rev 2008;88:1–35.
13. Gunning PW, Schevzov G, Kee AJ, Hardeman EC. Tropomyosin isoforms: divining rods for actin cytoskeleton function. Trends Cell Biol 2005;15:334–341.
14. McMichael BK, Kotadiya P, Singh T, Holliday LS, Lee BS. Tropomyosin isoforms localize to distinct microfilament populations in osteoclasts. Bone 2006;39:294–705.
15. Vlahovich N, Kee AJ, van der Poel C, Kettle E, Hernandez-Deviez D, Lucas C, Lynch GS, Parton RG, Gunning PW, Hardeman EC. Cytoskeletal tropomyosin Tm5NM1 is required for normal excitation-contraction coupling in skeletal muscle. Mol Biol Cell 2009;20:400–409.
16. Hook J, Lemckert F, Schevzov G, Fath T, Gunning P. Functional identity of the gamma tropomyosin gene: implications for embryonic development, reproduction and cell viability. Bioarchitecture 2011;1:49–59.
17. Chun K-H, Araki K, Jee Y, Lee D-H, Oh B-C, Huang H, Park KS, Lee SW, Zabolotny JM, Kim Y-B. Regulation of glucose transport by ROCK1 differs from that of ROCK2 and is controlled by actin polymerization. Endocrinology 2012;153:1649–1662.
18. Schevzov G, Bryce NS, Almonte-Baldonado R, Joya J, Lin JJ, Hardeman E, Weinberger R, Gunning P. Specific features of neuronal size and shape are regulated by tropomyosin isoforms. Mol Biol Cell 2005;16:3425–3437.
19. Ono S, Ono K. Tropomyosin inhibits ADF/cofilin-dependent actin filament dynamics. J Cell Biol 2002;156:1065–1076.
20. Bernstein BW, Bamburg JR. Tropomyosin binding to F-actin protects the F-actin from disassembly by brain actin-depolymerizing factor (ADF). Cell Motil 1982;2:1–8.
21. Ishikawa R, Yamashiro S, Matsumura F. Differential modulation of actin-severing activity of gelsolin by multiple isoforms of cultured rat cell tropomyosin. Potentiation of protective ability of tropomyosins by 83-kDa nonmuscle caldesmon. J Biol Chem 1989;264:7490–7497.
22. Tojkander S, Gateva G, Schevzov G, Hotulainen P, Naumanen P, Martin C, Gunning PW, Lappalainen P. A molecular pathway for myosin II recruitment to stress fibers. Curr Biol 2011;21:539–550.
23. Fanning AS, Wolenski JS, Mooseker MS, Izant JG. Differential regulation of skeletal muscle myosin-II and brush border myosin-I enzymology and mechanochemistry by bacterially produced tropomyosin isoforms. Cell Motil Cytoskeleton 1994;29:29–45.
24. Greenberg MJ, Ostap EM. Regulation and control of myosin-I by the motor and light chain-binding domains. Trends Cell Biol 2013;23:81–89.

25. Hodges AR, Krementsova EB, Bookwalter CS, Fagnant PM, Sladewski TE, Trybus KM. Tropomyosin is essential for processive movement of a Class V myosin from budding yeast. Curr Biol 2012;22:1410–1416.
26. Greeves MA, Hitchcock-Degregori SE, Gunning PW. A systematic nomenclature for mammalian tropomyosin isoforms. J Mus Res Cell Motil 2014; (In press) doi:10.1007/s10974-014-9389-6.
27. Pelham RJ, Lin JJ, Wang YL. A high molecular mass non-muscle tropomyosin isoform stimulates retrograde organelle transport. J Cell Sci 1996;109:981–989.
28. Clayton JE, Sammons MR, Stark BC, Hodges AR, Lord M. Differential regulation of unconventional fission yeast myosins via the actin track. Curr Biol 2010;20:1423–1431.
29. Kovar DR, Sirotkin V, Lord M. Three's company: the fission yeast actin cytoskeleton. Trends Cell Biol 2011;21:177–187.
30. Coulton AT, East DA, Galinska-Rakoczy A, Lehman W, Mulvihill DP. The recruitment of acetylated and unacetylated tropomyosin to distinct actin polymers permits the discrete regulation of specific myosins in fission yeast. J Cell Sci 2010;123:3235–3243.
31. Stark BC, Sladewski TE, Pollard LW, Lord M. Tropomyosin and myosin-II cellular levels promote actomyosin ring assembly in fission yeast. Mol Biol Cell 2010;21:989–1000.
32. Johnson M, East DA, Mulvihill DP. Formins determine the functional properties of actin filaments in yeast. Curr Biol 2014;24:1525–1530.
33. Kee AJ, Schevzov G, Nair-Shalliker V, Robinson CS, Vrhovski B, Ghoddusi M, Qiu MR, Lin JJC, Weinberger R, Gunning PW, Hardeman EC. Sorting of a nonmuscle tropomyosin to a novel cytoskeletal compartment in skeletal muscle results in muscular dystrophy. J Cell Biol 2004;166:685–696.
34. Schevzov G, Fath T, Vrhovski B, Vlahovich N, Rajan S, Hook J, Joya JE, Lemckert F, Puttur F, Lin JJC, Hardeman EC, Wieczorek DF, O'Neill GM, Gunning PW. Divergent regulation of the sarcomere and the cytoskeleton. J Biol Chem 2008;283:275–283.
35. Rowland AF, Fazakerley DJ, James DE. Mapping insulin/GLUT4 circuitry. Traffic 2011;12:672–681.
36. Ng Y, Ramm G, Lopez JA, James DE. Rapid activation of Akt2 is sufficient to stimulate GLUT4 translocation in 3T3-L1 adipocytes. Cell Metab 2008;7:348–356.
37. Ploug T, van Deurs B, Ai H, Cushman SW, Ralston E. Analysis of GLUT4 distribution in whole skeletal muscle fibers: identification of distinct storage compartments that are recruited by insulin and muscle contractions. J Cell Biol 1998;142:1429–1446.
38. Lauritzen HP, Ploug T, Prats C, Tavare JM, Galbo H. Imaging of insulin signaling in skeletal muscle of living mice shows major role of T-tubules. Diabetes 2006;55:1300–1306.
39. Lauritzen HP, Galbo H, Brandauer J, Goodyear LJ, Ploug T. Large GLUT4 vesicles are stationary while locally and reversibly depleted during transient insulin stimulation of skeletal muscle of living mice. Imaging analysis of GLUT4-EGFP vesicle dynamics. Diabetes 2007;57:315–324.
40. Lauritzen HP, Galbo H, Toyoda T, Goodyear LJ. Kinetics of contraction-induced GLUT4 translocation in skeletal muscle fibers from living mice. Diabetes 2010;59:2134–2144.
41. Stehn JR, Haass NK, Bonello T, Desouza M, Kottyan G, Treutlein H, Zeng J, Nascimento PRBB, Sequeira VB, Butler TL, Allanson M, Fath T, Hill TA, McCluskey A, Schevzov G, et al. A novel class of anticancer compounds target the actin cytoskeleton in tumor cells. Cancer Res 2013;73:5169–5182.
42. Stockli J, Fazakerley DJ, James DE. GLUT4 exocytosis. J Cell Sci 2011;124:4147–4159.
43. Tsakiridis T, Vranic M, Klip A. Disassembly of the actin network inhibits insulin-dependent stimulation of glucose transport and prevents recruitment of glucose transporters to the plasma membrane. J Biol Chem 1994;269:29934–29942.
44. Omata W, Shibata H, Li L, Takata K, Kojima I. Actin filaments play a critical role in insulin-induced exocytotic recruitment but not in endocytosis of GLUT4 in isolated rat adipocytes. Biochem J 2000;346:321–328.
45. Brozinick JT, Hawkins ED, Strawbridge AB, Elmendorf JS. Disruption of cortical actin in skeletal muscle demonstrates an essential role of the cytoskeleton in GLUT4 translocation in insulin sensitive tissues. J Biol Chem 2004;279:40699–40706.
46. Chiu TT, Patel N, Shaw AE, Bamburg JR, Klip A. Arp2/3- and cofilin-coordinated actin dynamics is required for insulin-mediated GLUT4 translocation to the surface of muscle cells. Mol Biol Cell 2010;21:3529–3539.
47. Balamatsias D, Kong AM, Waters JE, Sriratana A, Gurung R, Bailey CG, Rasko JEJ, Tiganis T, Macaulay SL, Mitchell CA. Identification of P-Rex1 as a novel Rac1-guanine nucleotide exchange factor (GEF) that promotes actin remodelling and GLUT4 trafficking in adipocytes. J Biol Chem 2011;286:43229–43240.
48. Chiu TT, Jensen TE, Sylow L, Richter EA, Klip A. Rac1 signalling towards GLUT4/glucose uptake in skeletal muscle. Cell Signal 2011;23:1546–1554.
49. Dominguez R. Tropomyosin: the gatekeeper's view of the actin filament revealed. Biophys J 2011;100:797–798.
50. McCarthy AM, Spisak KO, Brozinick JT, Elmendorf JS. Loss of cortical actin filaments in insulin-resistant skeletal muscle cells impairs GLUT4 vesicle trafficking and glucose transport. Am J Physiol Cell Physiol 2006;291:C860–C868.
51. Habegger KM, Penque BA, Sealls W, Tackett L, Bell LN, Blue EK, Gallagher PJ, Sturek M, Alloosh MA, Steinberg HO, Considine RV, Elmendorf JS. Fat-induced membrane cholesterol accrual provokes cortical filamentous actin destabilisation and glucose transport dysfunction in skeletal muscle. Diabetologia 2012;55:457–467.
52. Lim C-Y, Bi X, Wu D, Kim JB, Gunning PW, Hong W, Han W. Tropomodulin3 is a novel Akt2 effector regulating insulin-stimulated GLUT4 exocytosis through cortical actin remodeling. Nat Commun 2015;5:5951.
53. Randhawa VK, Ishikura S, Talior-Volodarsky I, Cheng AW, Patel N, Hartwig JH, Klip A. GLUT4 vesicle recruitment and fusion are differentially regulated by Rac, AS160 and RAB8A in muscle cells. J Biol Chem 2008;283:27208–27219.
54. Creed SJ, Desouza M, Bamburg JR, Gunning P, Stehn J. Tropomyosin isoform 3 promotes the formation of filopodia by regulating the

recruitment of actin-binding proteins to actin filaments. Exp Cell Res 2011;317:249–261.
55. McMichael BK, Lee BS. Tropomyosin 4 regulates adhesion structures and resorptive capacity in osteoclasts. Exp Cell Res 2008;314:564–573.
56. Bach CTT, Creed S, Zhong J, Mahmassani M, Schevzov G, Stehn J, Cowell LN, Naumanen P, Lappalainen P, Gunning PW, O'Neill GM. Tropomyosin isoform expression regulates the transition of adhesions to determine cell speed and direction. Mol Cell Biol 2009;29:1506–1514.
57. Yamashiro S, Gokhin DS, Kimura S, Nowak RB, Fowler VM. Tropomodulins: pointed-end capping proteins that regulate actin filament architecture in diverse cell types. Cytoskeleton (Hoboken, NJ) 2012;69:337–370.
58. Gokhin DS, Fowler VM. Cytoplasmic γ-actin and tropomodulin isoforms link to the sarcoplasmic reticulum in skeletal muscle fibers. J Cell Biol 2011;194:105–120.
59. Patel N, Huang C, Klip A. Cellular location of insulin-triggered signals and implications for glucose uptake. Pflugers Arch 2006;451:499–510.
60. Foley K, Boguslavsky S, Klip A. Endocytosis, recycling, and regulated exocytosis of glucose transporter 4. Biochemistry 2011;50:3048–3061.
61. McIntosh BB, Holzbaur ELF, Ostap EM. Control of the initiation and termination of kinesin-1-driven transport by myosin-1c and non-muscle tropomyosin. Curr Biol 2015;25:523–529.
62. Woody S, Stall R, Ramos J, Patel YM. Regulation of myosin light chain kinase during insulin-stimulated glucose uptake in 3T3-L1 adipocytes. PLoS One 2013;8:e77248.
63. Schevzov G, Whittaker SP, Fath T, Lin JJ, Gunning PW. Tropomyosin isoforms and reagents. Bioarchitecture 2011;1:135–164.
64. Novy RE, Sellers JR, Liu LF, Lin JJ. In vitro functional characterization of bacterially expressed human fibroblast tropomyosin isoforms and their chimeric mutants. Cell Motil Cytoskeleton 1993;26:248–261.
65. James DE, Strube M, Mueckler M. Molecular cloning and characterization of an insulin-regulatable glucose transporter. Nature 1989;338:83–87.
66. Wagner MC, Barylko B, Albanesi JP. Tissue distribution and subcellular localization of mammalian myosin I. J Cell Biol 1992;119:163–170.
67. Turner N, Bruce CR, Beale SM, Hoehn KL, So T, Rolph MS, Cooney GJ. Excess lipid availability increases mitochondrial fatty acid oxidative capacity in muscle: evidence against a role for reduced fatty acid oxidation in lipid-induced insulin resistance in rodents. Diabetes 2007;56:2085–2092.
68. Schevzov G, Gunning P, Jeffrey PL, Temm-Grove C, Helfman DM, Lin JJ, Weinberger RP. Tropomyosin localization reveals distinct populations of microfilaments in neurites and growth cones. Mol Cell Neurosci 1997;8:439–454.
69. Leong GM, Kee AJ, Millard SM, Martel N, Eriksson N, Turner N, Cooney GJ, Hardeman EC, Muscat GE. The Ski proto-oncogene regulates body composition and suppresses lipogenesis. Int J Obes (Lond) 2010;34:524–536.
70. Cooney GJ, Lyons RJ, Crew AJ, Jensen TE, Molero JC, Mitchell CJ, Biden TJ, Ormandy CJ, James DE, Daly RJ. Improved glucose homeostasis and enhanced insulin signalling in Grb14-deficient mice. EMBO J 2004;23:582–593.
71. Zisman A, Peroni OD, Abel ED, Michael MD, Mauvais-Jarvis F, Lowell BB, Wojtaszewski JFP, Hirshman MF, Virkamaki A, Goodyear LJ, Kahn CR, Kahn BB. Targeted disruption of the glucose transporter 4 selectively in muscle causes insulin resistance and glucose intolerance. Nat Med 2000;6:924–928.
72. Hom FG, Goodner CJ, Berrie MA. A [^{3}H]2-deoxyglucose method for comparing rates of glucose metabolism and insulin responses among rat tissues in vivo. Validation of the model and the absence of an insulin effect on brain. Diabetes 1984;33:141–152.
73. Garratt M, Pichaud N, Glaros EN, Kee AJ, Brooks RC. Superoxide dismutase deficiency impairs olfactory sexual signaling and alters bioenergetic function in mice. Proc Natl Acad Sci USA 2014;111:8119–8124.
74. Vlahovich N, Schevzov G, Nair-Shaliker V, Ilkovski B, Artap ST, Joya JE, Kee AJ, North KN, Gunning PW, Hardeman EC. Tropomyosin 4 defines novel filaments in skeletal muscle associated with muscle remodelling/regeneration in normal and diseased muscle. Cell Motil Cytoskeleton 2008;65:73–85.
75. French AP, Mills S, Swarup R, Bennett MJ, Pridmore TP. Colocalization of fluorescent markers in confocal microscope images of plant cells. Nat Protoc 2008;3:619–628.
76. Larance M, Ramm G, Stöckli J, van Dam EM, Winata S, Wasinger V, Simpson F, Graham M, Junutula JR, Guilhaus M, James DE. Characterization of the role of the Rab GTPase-activating protein AS160 in insulin-regulated GLUT4 trafficking. J Biol Chem 2005;280:37803–37813.
77. Shi J, Kandror K. Study of glucose uptake in adipose cells. In: Yang K, editor. Adipose Tissue Protocols. New York: Humana Press; 2008, pp. 307–315.
78. Pearen MA, Ryall JG, Lynch GS, Muscat GE. Expression profiling of skeletal muscle following acute and chronic beta2-adrenergic stimulation: implications for hypertrophy, metabolism and circadian rhythm. BMC Genomics 2009;10:448.
79. Manceva S, Lin T, Pham H, Lewis JH, Goldman YE, Ostap EM. Calcium regulation of calmodulin binding to and dissociation from the myo1c regulatory domain. Biochemistry 2007;46:11718–11726.
80. Lin T, Greenberg MJ, Moore JR, Ostap EM. A hearing loss-associated myo1c mutation (R156W) decreases the myosin duty ratio and force sensitivity. Biochemistry 2011;50:1831–1838.
81. Lin T, Tang N, Ostap EM. Biochemical and motile properties of Myo1b splice isoforms. J Biol Chem 2005;280:41562–41567.
82. Meijering E, Dzyubachyk O, Smal I. Methods for cell and particle tracking. Methods Enzymol 2012;504:183–200.